



Modeling the Impact of Tides and Geothermal Heat Flux on the Climate of Early Earth

Biewald, Benjamin; Green, Mattias; Petri, Stefan; Feulner, Georg

Paleoceanography and Paleoclimatology

DOI:

[10.1029/2024PA005016](https://doi.org/10.1029/2024PA005016)

Published: 10/12/2024

Peer reviewed version

[Cyswllt i'r cyhoeddiad / Link to publication](#)

Dyfyniad o'r fersiwn a gyhoeddwyd / Citation for published version (APA):

Biewald, B., Green, M., Petri, S., & Feulner, G. (2024). Modeling the Impact of Tides and Geothermal Heat Flux on the Climate of Early Earth. *Paleoceanography and Paleoclimatology*, 39(12). <https://doi.org/10.1029/2024PA005016>

Hawliau Cyffredinol / General rights

Copyright and moral rights for the publications made accessible in the public portal are retained by the authors and/or other copyright owners and it is a condition of accessing publications that users recognise and abide by the legal requirements associated with these rights.

- Users may download and print one copy of any publication from the public portal for the purpose of private study or research.
- You may not further distribute the material or use it for any profit-making activity or commercial gain
- You may freely distribute the URL identifying the publication in the public portal ?

Take down policy

If you believe that this document breaches copyright please contact us providing details, and we will remove access to the work immediately and investigate your claim.

Modelling the Impact of Tides and Geothermal Heat Flux on the Climate of Early Earth

Benjamin Biewald^{1,2}, J. A. Mattias Green³, Stefan Petri¹ and Georg Feulner^{1,2}

¹Earth System Analysis, Potsdam Institute for Climate Impact Research, Member of the Leibniz Association, Potsdam, Germany

²Institute of Physics and Astronomy, University of Potsdam, Potsdam, Germany

³School of Ocean Sciences, Bangor University, Menai Bridge, UK

Key Points:

- First spatially resolved modelling of both tides and their impact on early Earth's climate
- Impact of tidal heating is strongest when altering ocean surface currents close to the sea-ice edge
- Tidal heating has only local impacts, but tidal mixing and geothermal heat flux influence global climate state

Corresponding author: Georg Feulner, feulner@pik-potsdam.de

Corresponding author: J. A. Mattias Green, m.green@bangor.ac.uk

Abstract

On early Earth increased rates of tidal energy dissipation are likely, but depend on the (unknown) distribution of continents. A stronger tidal heating could provide an additional energy source during times of substantially lower solar input. So far, the problem has been assessed in terms of the negligible contribution to Earth’s global energy budget. Here we present a spatially resolved investigation of the impact of tidal heating, mixing, and geothermal heat on early Earth’s climate. Using a random landmass distribution, tidal heating is calculated for three different rotation periods (12, 18, 24 hours) and fed into a climate model. For each rotation rate, three climate states with different atmospheric CO₂ levels are simulated. We find that, depending on the climate state, tidal heating can affect regional ocean dynamics and sea-ice cover. The impact is strongest when tidal heating alters sea-ice dynamics and meridional heat transport close to the sea-ice edge, but its global impact remains negligible with only small global mean changes in ice cover ($\sim 0.3\%$) and temperature ($< 0.05^\circ\text{C}$). Adding tidal mixing and geothermal heat, however, leads to significant reduction in sea-ice cover of $\sim 11\%$ and $\sim 19\%$, respectively, and thus to larger global warming. As we do not consider the dynamical effects of a higher rotation rate or different landmass distributions, this is only a first glimpse at the importance of tides for the climate of early Earth. Nevertheless, our results suggest that tides and geothermal heat are important for understanding regional climates and could have contributed to warming early Earth.

1 Introduction

Ocean tides influence a range of key Earth system processes (Green & Duarte, 2022). These include sustaining ocean primary production (Sharples et al., 2007; Tuerena et al., 2019), providing parts of the energy needed to maintain the climate-regulating overturning circulation in the ocean (Wunsch & Ferrari, 2004; Wilmes et al., 2021), and contributing to key evolution events (Balbus, 2014; Byrne et al., 2020). The drag introduced on Earth by the tides also forces Earth’s spin to slow down, increasing day length, and causing the Moon to recede to conserve angular momentum of the system (MacDonald, 1964; Bills & Ray, 1999; Daher et al., 2021). Consequently, on early Earth the Moon was closer and the days much shorter. The Archean Eon spans nearly 1/3 of Earth’s history – from 4000–2500 Ma (million years ago) – and there is naturally uncertainty and a range of estimates of daylength for the Eon, from as short as 13 hours at 3200 Ma (Eulendorf & Heubeck, 2023) to 18 hours at the end of the Eon (Farhat et al., 2022; Daher et al., 2021). The tides are consequently the key controller of day length, which directly influence planetary habitability (Yang et al., 2014) as well as the timing of the oxygenation of the atmosphere (Klatt et al., 2021). An understanding of the evolution of tides and tidal drag through Earth’s history is therefore key to understand other Earth system events.

The first order controller of tidal energetics is continental configuration, as for a fixed lunar distance, and hence tidal forcing, the tidal dissipation rates can vary up to three orders of magnitudes depending on continental configuration (Green et al., 2017; Blackledge et al., 2020). Consequently, even though the forcing was larger during the Archean, the tides may not have been more energetic. This is because the tides become resonant for specific basin geometries (Green, 2010), e.g., the present day North Atlantic (Egbert et al., 2004; Green, 2010), and that effect can lead to larger amplification of the tide than the increase in forcing alone can do (Green et al., 2020).

The influence of the tides on the climate of Early Earth has largely been assessed in terms of their contribution to the planetary energy balance (Barnes et al., 2008) in light of the Faint Young Sun Problem (FYSP) (Feulner, 2012). Even considering the larger tidal forcing on early Earth and the uncertainty with respect to continental configuration, however, the heating from tidal dissipation is expected to be negligible compared to the energy input from the faint young Sun. Nevertheless, recent investigations of the

geological imprint of ancient tides and the long-term evolution of the Earth-Moon distance have led to a renewed interest in the potential influence of tidal heating on the Hadean and Archean climate. For example, based on simple models for the long-term evolution of Earth’s tides, Heller et al. (2021) argue that the global tidal dissipation, and hence heating, rate on early Earth may have been underestimated. They conclude that tides might have helped to keep surface water liquid for 220 Myr and could thus have been an important contribution to the planetary energy budget during the early Hadean. However, their approach necessarily neglects both tidally driven ocean dynamics and the influence of continental configuration on tidal dissipation (and is thus mainly a valid representation of deep aquaplanets), and the climatic consequences are assessed with a zero-dimensional grey atmosphere model ignoring internal climate dynamics and the ice-albedo feedback.

Here, we take the first step towards a more comprehensive assessment of the impact of tides on early Earth’s climate by computing tidal energy dissipation rates from a spatially resolved tidal model for one particular continental configuration (broadly representative of an early Earth) and feeding the additional energy input as heat into a three-dimensional coupled climate model. This way, we can also investigate the effect of local tidal heating on ocean and sea-ice dynamics beyond the negligible impact on the global climate. Furthermore, we run additional sets of simulations including the effects of tides on vertical mixing in the ocean and with geothermal heat flux.

2 Methods

2.1 Tidal Modelling

The tide model simulations were done using OTIS, the Oregon State Tidal Inversion Software (e.g., Egbert et al., 2004; Green & Nycander, 2013). It has been used extensively for paleotidal simulations as far back as the Proterozoic (Green & Huber, 2013; Green et al., 2017; Green et al., 2020; Green & Duarte, 2022). It solves the linearised shallow water equations:

$$\frac{\partial \mathbf{U}}{\partial t} + \mathbf{f} \times \mathbf{U} = -gH\nabla(\zeta - \zeta_{EQ} - \zeta_{SAL}) - \mathbf{F} \quad (1)$$

$$\frac{\partial \zeta}{\partial t} = -\nabla \cdot \mathbf{U} \quad (2)$$

Here, \mathbf{U} is the depth integrated volume transport, H is water depth, \mathbf{f} the Coriolis vector, g the gravitational constant, ζ the tidal elevation, ζ_{EQ} the equilibrium tidal elevation, and ζ_{SAL} the tidal elevation due to self-attraction and loading. The tidal drag is parameterised through two parts: $\mathbf{F} = \mathbf{F}_B + \mathbf{F}_{IT}$, where \mathbf{F}_B is frictional losses due to bed friction and \mathbf{F}_{IT} energy losses due to tidal conversion. The former is represented by the standard quadratic law:

$$\mathbf{F}_B = C_d \mathbf{u} |\mathbf{u}| \quad (3)$$

where $C_d = 0.003$ is a drag coefficient, and \mathbf{u} tidal velocity. The conversion is written as $\mathbf{F}_{IT} = C_{IT} \mathbf{U}$, with the conversion coefficient C_{IT} given by (Zaron & Egbert, 2006; Green & Nycander, 2013)

$$C_{IT}(x, y) = \gamma \frac{(\nabla H)^2 N_b \bar{N}}{8\pi\omega} \quad (4)$$

where $\gamma = 50$ is a scaling factor (see Zaron & Egbert, 2006, for more details), N_b the buoyancy frequency at the sea-bed, \bar{N} the vertical average of the buoyancy frequency, and ω is the frequency of the tidal constituent under evaluation. The buoyancy frequency is computed from a statistical fit based on observations from present day Earth, or $N(x, y) = 0.00524 \exp(-z/1300)$, where z is the vertical coordinate, and the constants 0.00524 and 1300 have units of s^{-1} and m, respectively. Whilst the abyssal stratification is known from the climate model simulations (see section 2.3), the tides are relatively insensitive

113 to changes in stratification within a factor 2 (Egbert et al., 2004). Furthermore, itera-
 114 tive studies, where stratification has been implemented in the tidal model and the re-
 115 sulting dissipation returned to a climate model, showed only minor impact on the results
 116 (Schmittner et al., 2015).

117 2.2 Simulations and Computations

118 The tidal dissipation rates, D , were computed using the energy balance method
 119 (Egbert & Ray, 2001)

$$D = W - \nabla \cdot \mathbf{P} \quad (5)$$

120 The work rate done by the tide-generating force, W , and the energy flux, \mathbf{P} , are given
 121 by

$$W = g\rho_0 \langle \mathbf{U} \cdot \nabla (\eta_{eq} + \eta_{SAL}) \rangle \quad (6)$$

$$\mathbf{P} = g\rho_0 \langle \mathbf{U} \eta \rangle \quad (7)$$

124 in which $\langle \rangle$ denote time-averages over a tidal period. As the end result of tidal energy
 125 dissipation is heat, we add the tidal dissipation as tidal heating in the climate model.

126 Tidal model simulations were done for three rotation rates – 12, 18, and 24 hours
 127 – using one topography – denoted “225” – from Blackledge et al. (2020). This was cho-
 128 sen because it consists of a series of smaller continents scattered around the planet, much
 129 like early Earth has been proposed to have looked like (Hawkesworth et al., 2020; Sawada,
 130 2020; Cawood et al., 2022). The associated changes in tidal forcing due the closer prox-
 131 imity of the Moon for each investigated rotation rate was taken from Daher et al. (2021).
 132 The resulting tidal energy dissipation fields are shown in Fig. 1.

133 2.3 Modelling Tidal Impacts on Early Earth’s Climate

134 To investigate the impact of tidal energetics on the climate on early Earth, we em-
 135 ploy the deep-time version of the intermediate-complexity climate model CLIMBER-3 α
 136 (Montoya et al., 2005). The model is based on a modified version of the ocean general
 137 circulation model MOM3 (Pacanowski & Griffies, 1999; Hofmann & Morales Maqueda,
 138 2006) run at a horizontal resolution of $3.75^\circ \times 3.75^\circ$ and using 24 levels vertically, a sea-
 139 ice model capturing both thermodynamics and dynamics (Fichefet & Morales Maqueda,
 140 1997) at the same horizontal resolution as the ocean model, and a fast statistical-dynamical
 141 atmosphere model (Petoukhov et al., 2000) with a coarse horizontal resolution of 22.5°
 142 in longitude and 7.5° in latitude. The deep-time version of CLIMBER-3 α entails the re-
 143 moval of parameterisations relating to the present-day climate system, additional diag-
 144 nostics, and bug fixes. This version has been used in a range of studies relating to plan-
 145 etary habitability, in particular for the climate on early Earth (Kienert et al., 2012, 2013)
 146 and major glaciations in Earth’s history (Feulner & Kienert, 2014; Feulner et al., 2015;
 147 Feulner, 2017; Eberhard et al., 2023; Feulner et al., 2023).

148 All climate model simulations are run for the continental configuration “225” from
 149 Blackledge et al. (2020) as described above, re-gridded to the resolution of the ocean model
 150 (see Fig. 2). The solar constant values corresponding to the three tidal scenarios with
 151 12, 18, and 24 hours rotation rate are computed based on the relation between day length
 152 and time from Farhat et al. (2022) and the stellar evolution model MESA (Jermyn et
 153 al., 2023). For each rotation rate, simulations with three different atmospheric CO₂ lev-
 154 els are performed which are characterised by a low, medium, and high fraction of global
 155 sea-ice cover (see Table 1). We run four sets of nine simulations each:

- 156 1. *Control simulations* for the three tidal scenarios and three climate states without
 157 any tidal effects and ignoring geothermal heat flow. Key ocean and sea-ice char-
 158 acteristics of these simulations are shown in Figure B1 in Appendix B.

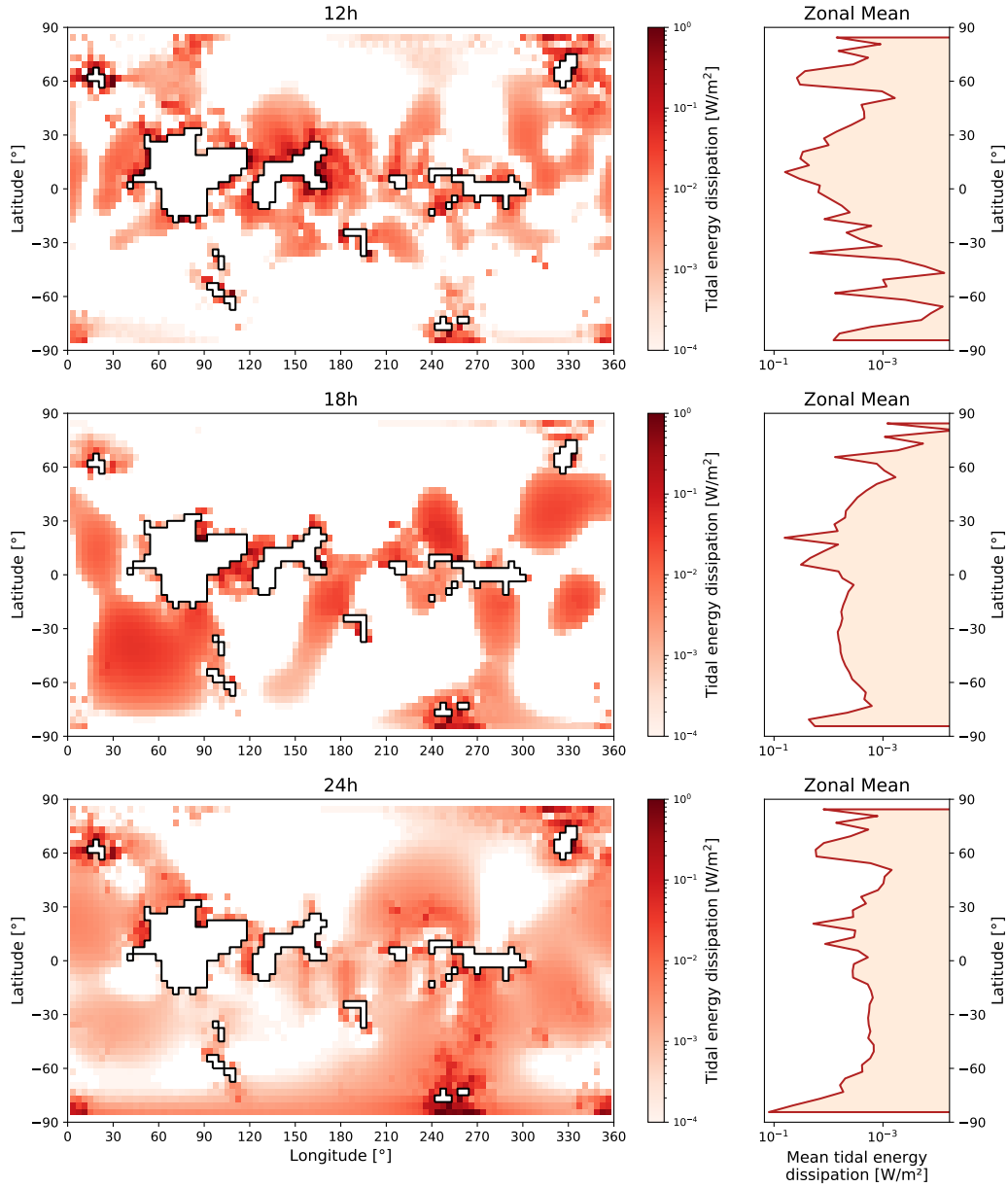


Figure 1. Maps (left column) and zonal means (right column) of modelled tidal dissipation rates for all three rotation rates of 12 h (top panels), 18 h (middle panels), and 24 h (bottom panels). Note the logarithmic scale.

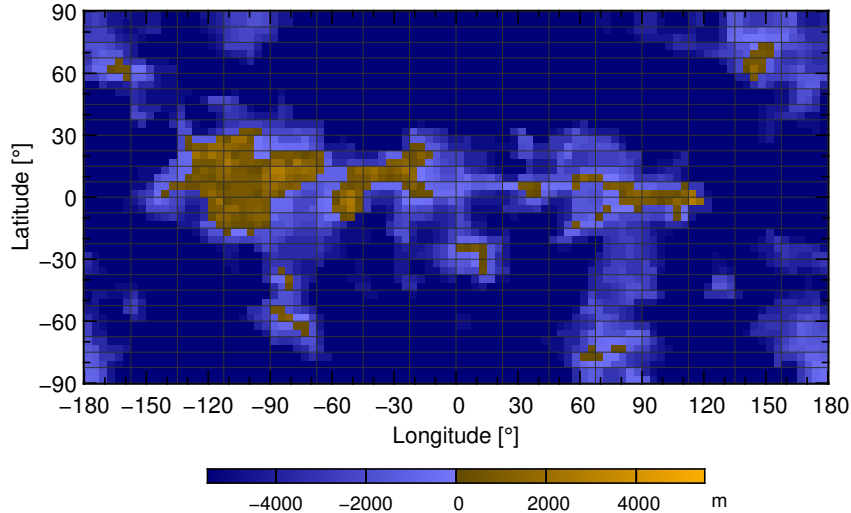


Figure 2. Ocean bathymetry and land orography based on continental configuration “225” from Blackledge et al. (2020) at the $3.75^\circ \times 3.75^\circ$ resolution of CLIMBER-3 α ’s ocean model.

- 159
- 160
- 161
- 162
- 163
- 164
- 165
- 166
- 167
- 168
- 169
- 170
- 171
- 172
- 173
- 174
- 175
- 176
- 177
- 178
- 179
- 180
- 181
- 182
- 183
- 184
- 185
- 186
- 187
- 188
- 189
- 190
2. Same as 1., but including the effects of *tidal heating*. In this case, the energy input by the tides (computed as described in Sections 2.1 and 2.2, and shown in Fig. 1) is implemented as additional bottom heat flux into the ocean.
 3. Same as 2., but taking the *effects of tides on vertical mixing* into account. The vertical diffusivity is represented in the model by a constant background diffusivity, **afkph**, and an amplitude of the spatially varying diffusivity, **dfkph**. In the control simulations these are tuned to present day values of 0.8×10^{-4} and $1.05 \times 10^{-4} \text{ m}^2 \text{ s}^{-1}$, respectively. At present day the energy required to sustain abyssal diffusivities is provided in equal parts by the wind and the tide (Wunsch & Ferrari, 2004), and we assumed the same ratio here. For simplicity, we computed the ratio, R , of the globally integrated abyssal tidal dissipation rates (i.e., in waters deeper than 500 m) from the simulations presented here to a present-day tidal model simulation (Green et al., 2017), i.e., $R = D_{\text{Archaean}}/D_{\text{PD}}$. We then modify the tidally driven half of the **afkph** and **dfkph** by multiplying the control value with R so that **afkph** = $0.8 \times (0.5 + 0.5R)$ and **dfkph** = $1.05 \times (0.5 + 0.5R)$. The resulting values are shown in Table 2 and further highlight the existing knowledge that tidal dissipation rates, and hence vertical mixing, are to first order controlled by continental configuration (Blackledge et al., 2020; Green et al., 2018). The dissipation and associated diffusivity change by around 20% when we move from a present day topography (24 hour control) to our chosen Archean one (24 hour Archean). The reason for this is tidal resonances developing over large areas in the Archean topography. As we then change rotation rate, the Archean basins go out of resonances for an 18 hour day length; coincidentally the background diffusivity is then the same as for present day. At 12 hours, the tides become more energetic and the diffusivity is 80% higher than at present. Note that Farhat et al. (2022) propose a rapid change in day length between 12–15 hours due to potential orbital resonances and our results support this. Also note that because the diffusivity is computed in waters deeper than 500 m and the tidal heating is the total dissipation, including shallow waters we can have the same total dissipation but different diffusivities and vice versa.
 4. Same as 3., but *adding geothermal heat flux*. Time evolution of global geothermal heat flux from radioactive decay follows Turcotte and Schubert (2002), with the

Table 1. Overview of tidal scenarios and climate model simulations. Tidal simulations are performed for three different day lengths; the corresponding point in time is estimated from day length following Farhat et al. (2022), the value of the solar constant S_0 at these times are obtained from stellar evolution model MESA (Jermyn et al., 2023). The corresponding global mean values for tidal heating (from the tidal model) and geothermal heating (see text for details) are indicated as well. For each of the three tidal scenarios, climate model simulations are performed at three atmospheric CO₂ concentrations for which the climate model simulations yield low, intermediate, and high global sea-ice cover.

Day length [h]	Time [Myr]	Age [Ma]	S_0 [W/m ²]	Tidal heating [mW/m ²]	Geothermal [mW/m ²]	CO ₂ [ppm]	Ice cover
12	867	3700	1010	14.40	217.7	176,000	16%
						200,000	7.1%
						220,000	3.0%
18	2767	1800	1161	10.90	121.6	15,000	15%
						25,000	5.4%
						28,000	3.2%
24	4567	0	1361	2.758	90.42	140	14%
						277	7.2%
						350	4.5%

191 surface heat flow due to mantle cooling adjusted to 29 mW/m² to yield a present-
 192 day flux of 87 mW/m² for the modern continental configuration (Pollack et al.,
 193 1993). Furthermore, values are multiplied by a factor of 1.03 to take the partition-
 194 ing between continental and oceanic crust for the lower total land area of conti-
 195 nental configuration “225” into account. As for tidal heating, geothermal heat flux
 196 is uniformly distributed over the globe and added to the lowermost ocean cells;
 197 input to land areas is ignored in the model.

198 We employ an idealised present day-like orbital configuration with an obliquity of
 199 23.5° and a circular orbit. All climate model simulations were integrated for at least 4000
 200 years until equilibrium was approached. Note that rotation rates in the climate model
 201 simulations are 24 hours throughout to isolate the effect of tidal dissipation on the cli-
 202 mate from the changes in Earth-system dynamics due to higher rotation rates (which
 203 are beyond the scope of this paper).

204 3 Results

205 In the following, we will look at the impact of tidal heating, tidal mixing, and geother-
 206 mal heat flux on the climate for the different sets of simulations described in Section 2.3
 207 by comparing the changes in key climate variables, in particular surface air temperature
 208 (SAT), sea-surface temperature (SST), sea-ice cover, and ocean surface velocities com-
 209 pared to the respective control simulations (the latter are shown in Figure B1). All di-
 210 agnostics have been averaged over the last 500 years of each simulation to minimise the
 211 impact of inter-annual to centennial climate variability. With respect to the overall cli-
 212 mate state, the global and annual mean SATs and SSTs of all simulations are summarised
 213 in Table A1. We structure the discussion of results of our simulation experiments fol-
 214 lowing three key messages summarising the dependence on rotation rate (Section 3.1,
 215 Figure 3), climate state (Section 3.2, Figure 4), and forcing (Section 3.3, Figures 5 and
 216 6).

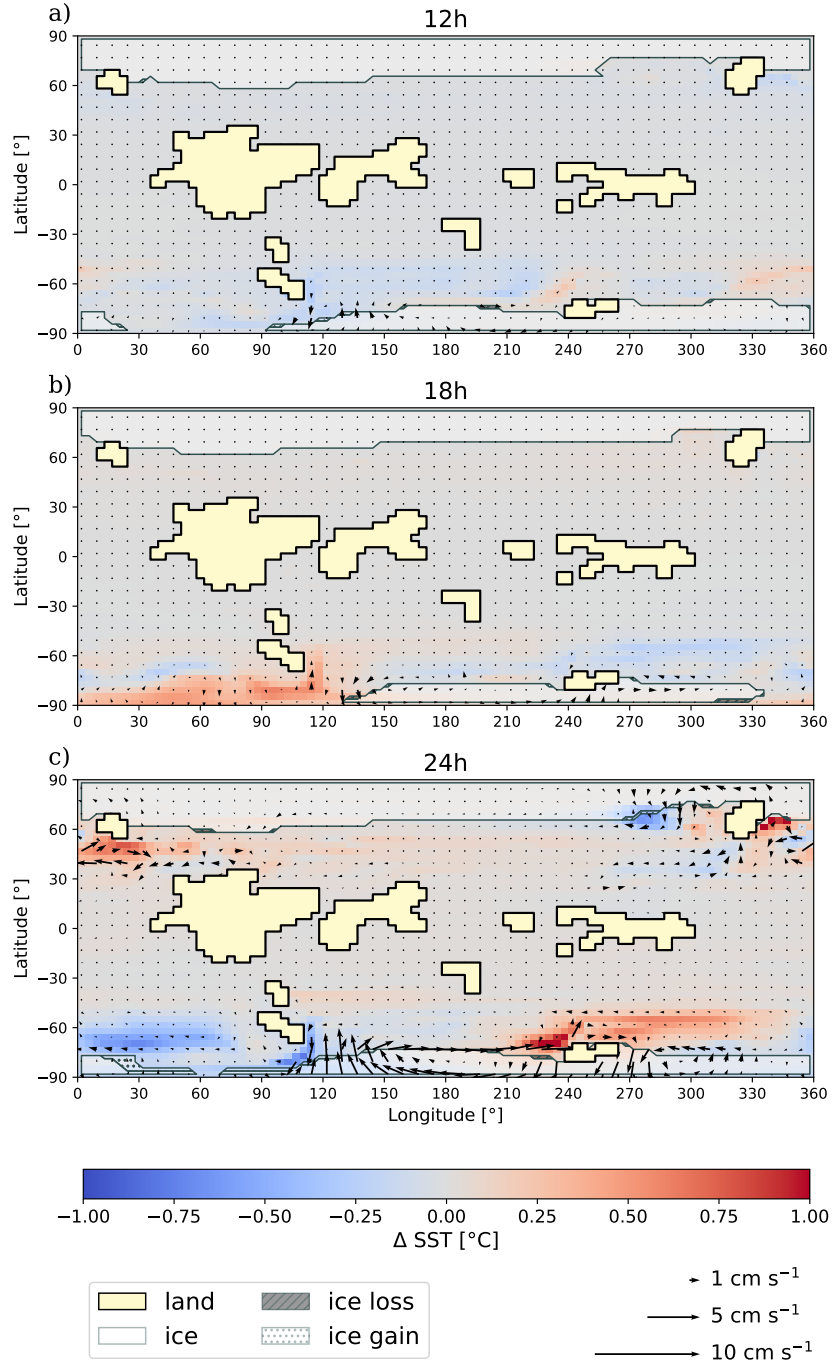


Figure 3. Tidal heating and climate-system response depend on rotation rate. Changes in sea-surface temperature, surface velocity, and sea-ice cover due to tidal heating for three different tidal scenarios with (a) 12 h, (b) 18 h, and (c) 24 h rotation rate and for intermediate CO₂ levels. The blue and red colors correspond to changes in SST when introducing tidal heating. Yellow areas are land; semi-transparent white areas correspond to regions that have at least 50% sea-ice fraction in the annual mean. Dotted and hatched areas represent regions of sea-ice gain or loss, respectively. Arrows indicate a change in ocean surface currents, with their length scaling with the change in speed. Maps showing the effects of tidal heating for all climate states and all rotation rates can be found in Figure B2 in Appendix B.

Table 2. Summary of the background (**afkph**) and amplitude (**dfkph**) of the vertical diffusivities used in the simulations; the 24 h values are the present-day default values used in the coupled climate model.

Day length [h]	afkph [$10^{-4} \text{ m}^2 \text{ s}^{-1}$]	dfkph [$10^{-4} \text{ m}^2 \text{ s}^{-1}$]
12, Archean	1.44	1.90
18, Archean	0.80	1.05
24, Archean	0.96	1.26
24, control	0.80	1.05

3.1 Climate response to tidal heating depends on rotation rate

For a given continental configuration, tidal dissipation (and thus heating) strongly depends on the assumed daylength (see Figure 1). These differences in tidal dissipation are also reflected in the climate response to this heating shown in Figure 3 for the intermediate climate state (the corresponding maps for all climate states can be found in Figure B2 in Appendix B). Although the global effect of tidal heating on the climate is very small (with global annual mean surface air temperature changes typically less than 0.1°C , see Table A1), marked regional impacts are visible at higher latitudes, varying with the spatial distribution and magnitude of tidal heating for different rotation rates.

These changes in sea-surface temperature, sea-ice cover, and ocean surface velocities in Figure 3 are largest close to the sea-ice edge and suggest that the response is (at least partly) mediated through changes in ocean currents. In our simulations, tidal heating impacts regional SST mostly by altering ocean surface currents and hence sea-ice dynamics as well as meridional heat transport. Depending on the patterns of the ocean surface currents and the sea-ice extent, tidal heating can have varying regional impacts. In particular, it is important to note that patterns of tidal heating do not necessarily correlate with regions of surface warming, as the tidal heat itself is too weak to penetrate to the surface and cause substantial changes in sea-ice cover (see below). Instead, the heating leads to changes in ocean surface currents which can trigger retreat or even advance of sea ice and thus local warming or cooling, respectively.

3.2 Climate response to tidal heating depends on background climate

The observation from Section 3.1 that tidal heating has the most significant effect on the climate if it can influence the sea-ice edge also leads to a strong dependence of the response to the background climate state, see Figure 4 for a rotation rate of 12 hours, and Figure B2 for all rotation rates and climate states.

Cold climate states with a large sea-ice extent experience hardly any impact of tidal heating on the ice cover. This is not too surprising, because the minute tidal warming mostly occurs at depth (see also Figure 7a), and because the extended sea-ice cover impedes strong meridional surface currents and heat exchange between the ocean and the atmosphere in the polar regions. Instead sea-ice cover reaches down to latitudes of roughly 50°N/S , respectively, where ocean surface currents are mostly zonal for the continental configuration used in our study (see Figure B1 in Appendix B) and thus do not greatly contribute to meridional heat transport towards the sea-ice edge.

Intermediate and warm climate states, on the other hand, show more pronounced impacts of tidal heating on sea-ice cover, as tidal heating influences ocean surface currents close to the sea-ice edge in this case, leading to changes in sea-ice cover and thus

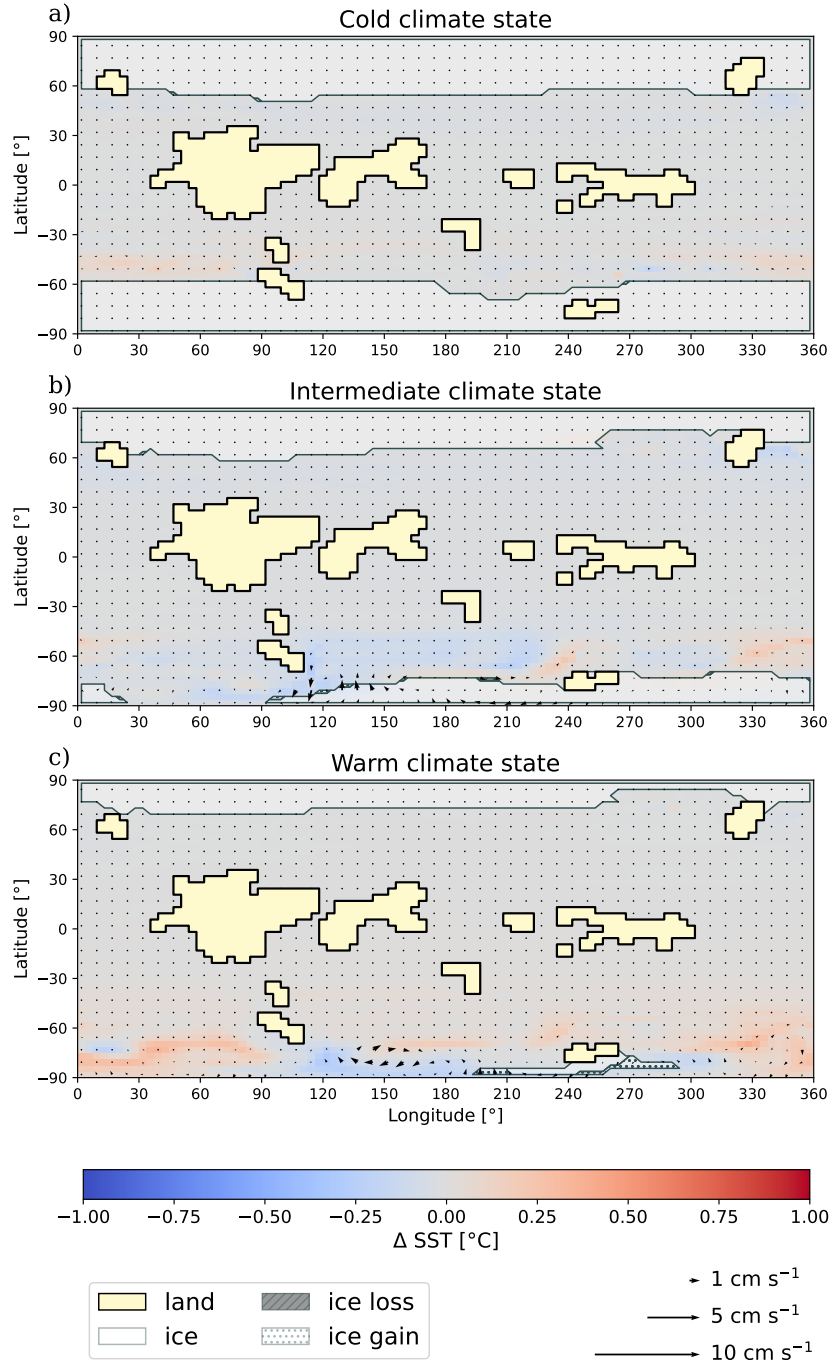


Figure 4. Response to tidal heating depends on background climate state. Changes in sea-surface temperature, surface velocity, and sea-ice cover due to tidal heating for a (a) cold, (b) intermediate, and (c) warm climate state and for a rotation rate of 12 h. See caption of Figure 3 for explanation of colors and shading. Maps showing the effects of tidal heating for all rotation rates can be found in Figure B2 in Appendix B.

253 local climate, amplified by the ice-albedo feedback. Despite the fact that tidal heating
 254 is a source of energy to the ocean, the effects on SST and sea-ice extent by tidal heat-
 255 ing can lead to either regional warming or cooling depending on how ocean surface cur-
 256 rents are affected. This also strongly depends on the continental configuration, of course.
 257 For example, the shape, position, and orientation of the islands at high southern lati-
 258 tudes leads to flow of warmer surface waters towards the polar region, significantly af-
 259 fecting local sea-ice cover. The distribution of continents is also responsible for the North-
 260 South asymmetry in the response to tidal heating: There is slightly more land in the South-
 261 ern hemisphere leading to an enhanced dissipation and tidal heating closer to the ocean
 262 surface (see Figure 7a) and to an offset in the global overturning circulation (see Fig-
 263 ure 8a). It is therefore worth noting that even a small asymmetry in continental config-
 264 uration can lead to significant differences in the state of the ocean. In general, climate
 265 states with strong meridional surface currents near the sea-ice edge are more vulnera-
 266 ble to changes in ocean circulation. The impact of tidal heating is therefore strongest
 267 in these cases.

268 **3.3 Tidal mixing and geothermal heat are more important than tidal** 269 **heating**

270 Despite the regional variations described above, the global impact of tidal heating
 271 on surface air temperatures, SSTs, and sea-ice cover is almost negligible, at least for the
 272 investigated continental configuration, tidal scenarios, and climate states. Tidally induced
 273 changes in global mean surface air temperatures vary between -0.022°C and $+0.035^{\circ}\text{C}$,
 274 depending on tidal scenario and baseline state (for comparison, the standard deviation
 275 of the global mean temperature due to natural climate variability in the control simu-
 276 lations ranges from 0.003°C to 0.048°C). The mean difference in global sea-ice over all
 277 scenarios and states is about $+8.6 \times 10^4 \text{ km}^2$ equivalent to a very small gain of 0.25%
 278 of the total sea-ice area.

279 As we have seen in Section 3.2, for a cold climate state and 12 hour rotation rate,
 280 for example, the influence of tidal heating is insignificant in the case of the cold climate
 281 state (Figures 4a and 5a) with the global and annual mean surface air temperature re-
 282 maining the same as for the control simulation (9.2°C). The reason becomes obvious when
 283 looking at the temperature distribution with depth and latitude (Figure 7a). As the tidal
 284 heating is small (fractions of a W m^{-2}), the heat itself is not large enough to penetrate
 285 to the ocean surface and directly influence SSTs unless the energy input occurs close to
 286 the ocean surface. In some regions, the energy input from tidal heating leads to a small
 287 warming at depth, other regions show slight cooling due to changes in ocean circulation.
 288 In general, these temperature changes are small ($|\Delta T| < 0.05^{\circ}\text{C}$) and cannot signifi-
 289 cantly affect the surface climate. Furthermore, tidal heating does not significantly change
 290 the amplitude or structure of the global overturning (see Figure 8a–b).

291 The response of the climate to tides changes significantly when taking the effect
 292 of tidal mixing into account in addition to just tidal heating (see Figures 5b and 6b for
 293 the cold and warm climate state, respectively). In this case, the global climate is signif-
 294 icantly warmer, with a global and annual mean surface air temperature of 10°C com-
 295 pared to 9.2°C in the control simulation for the cold climate state. Generally speaking,
 296 tidally enhanced ocean mixing will transport the tidal heat from the deeper ocean lay-
 297 ers towards the surface and can thus affect the surface climate either directly or via changes
 298 in ocean currents or sea-ice cover, amplified by the ice-albedo feedback. This effect can
 299 clearly be seen in the depth-latitude temperature section (Figure 7b). For all climate states
 300 and rotation rates, the changes in global and annual mean surface air temperatures com-
 301 pared to the respective control simulations range from -0.013°C to $+0.72^{\circ}\text{C}$ when tidal
 302 mixing is included. Global sea-ice area changes by about $-3.8 \times 10^6 \text{ km}^2$, equivalent to
 303 a loss of 11% of the total sea-ice area of the corresponding control simulation.

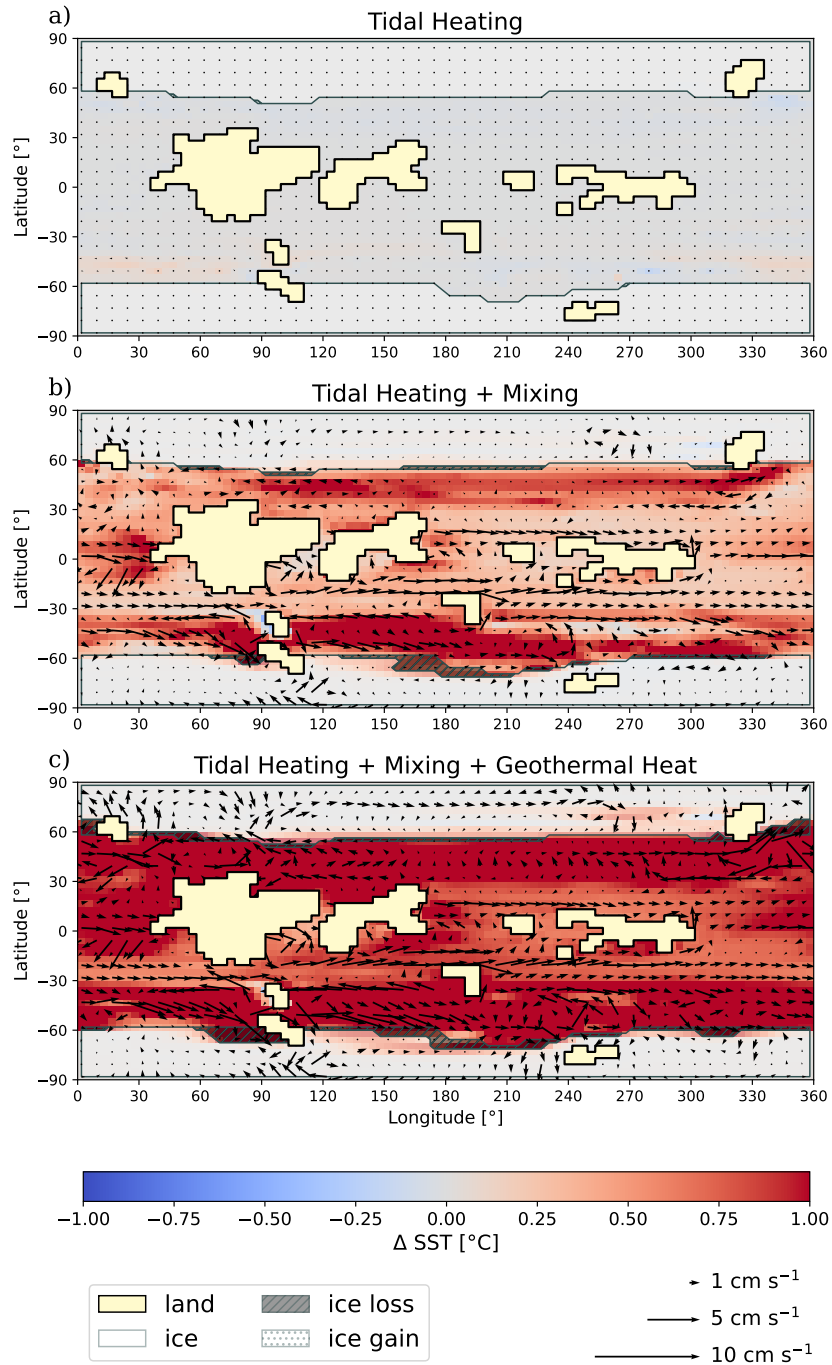


Figure 5. Tidal mixing and geothermal heat flow are more important than tidal heating (cold climate state). Changes in sea-surface temperature, surface velocity, and sea-ice cover for a cold climate state with 12h rotation rate and due to (a) tidal heating only, (b) tidal heating and mixing, and (c) tidal heating, mixing, and geothermal heat flow. See caption of Figure 3 for explanation of colors and shading. Appendix B contains all maps showing the effects of tidal heating (Figure B2), tidal heating and mixing (Figure B3), and tidal heating, mixing, and geothermal heat flux (Figure B4), respectively.

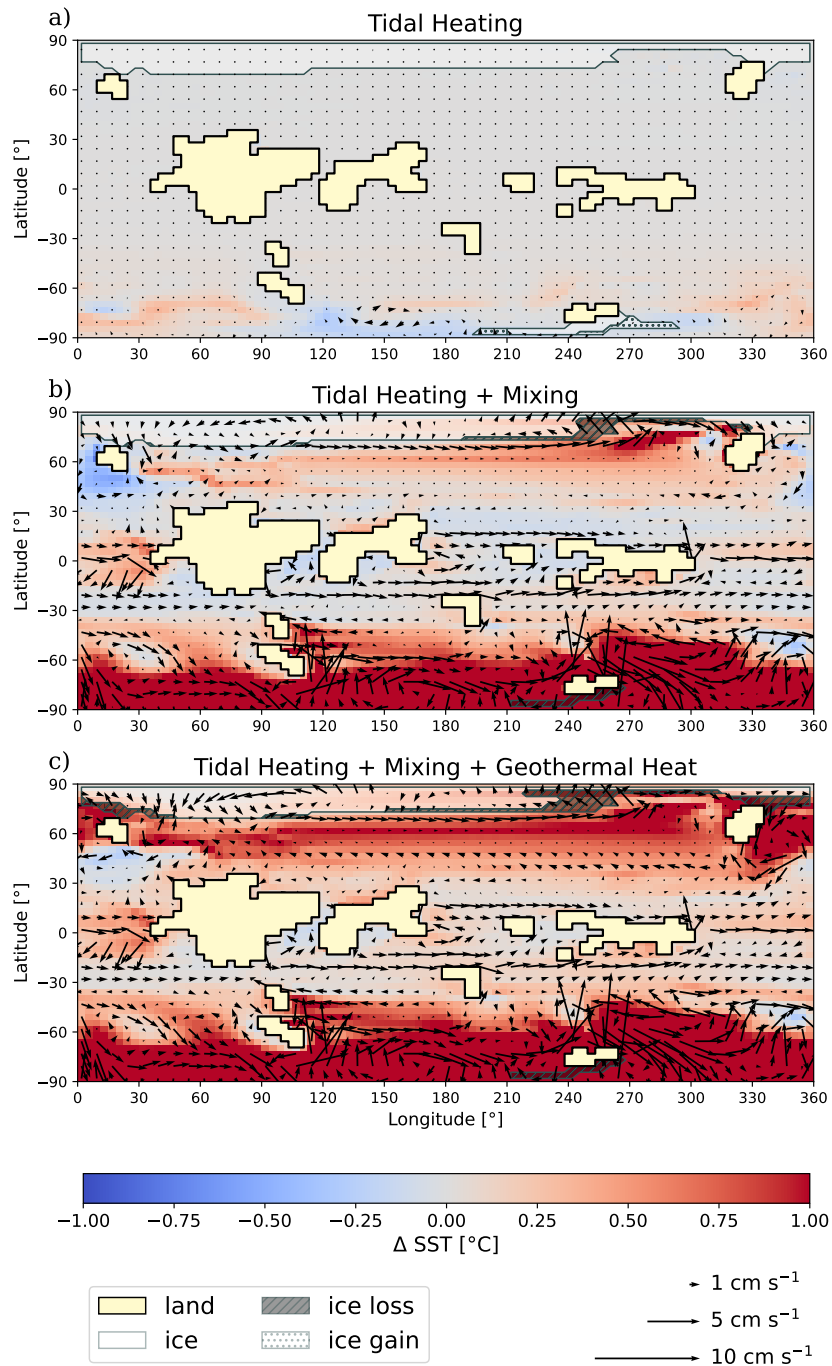


Figure 6. Tidal mixing and geothermal heat flow are more important than tidal heating (warm climate state). Same as Figure 5 but for a warm climate state. Appendix B contains all maps showing the effects of tidal heating (Figure B2), tidal heating and mixing (Figure B3), and tidal heating, mixing, and geothermal heat flux (Figure B4), respectively.

304 Adding geothermal heat flux on top of tidal heating and mixing leads to even more
 305 pronounced changes in the surface climate (see Figures 5c and 6c for the cold and warm
 306 climate state, respectively), with global mean surface air temperature changes relative
 307 to the control simulations in the range of $+0.13^{\circ}\text{C}$ to $+1.7^{\circ}\text{C}$ depending on the tidal sce-
 308 nario and climate state. The mean change in sea-ice area is also more pronounced in this
 309 case, about $-6.9 \times 10^6 \text{ km}^2$, equivalent to a loss of 19% of the total sea-ice area in the
 310 control simulations. The more pronounced response is hardly surprising given that the
 311 geothermal heat flux is one order of magnitude larger than the tidal heating (see Table 1).
 312 For the cold climate case, for example, the global and annual mean surface air temper-
 313 ature increases to 11°C , and thus 1.0°C higher than for the simulation with tidal heat-
 314 ing plus mixing or 1.8°C higher than the control simulation. Compared to the simula-
 315 tion with tidal heating, the input of heat is more uniform and generally at larger depths,
 316 leading to an overall warming of the ocean on top of the changes induced by tidal heat-
 317 ing and mixing (see Figure 7c).

318 The global overturning streamfunction (Figure 8) shows a northern hemisphere clock-
 319 wise cell with a maximum of about 25 Sv between $60\text{--}70^{\circ}\text{N}$. This shows that deepwater
 320 forms in the north and spreads out at depth, much like in the present day North Atlantic.
 321 There is a corresponding counter-clockwise cell in the southern hemisphere, but it is much
 322 weaker than the cell in the north in the control and tidal heating runs (Figure 8a–b). As
 323 tidal mixing is included, the southern cell becomes more energetic, and with all tidal pro-
 324 cesses and geothermal heat switched on (Figure 8d) there is a deep cell in the southern
 325 hemisphere with a maximum of some 20 Sv between $30\text{--}70^{\circ}\text{S}$. It has been known for some
 326 time that the strength of the overturning circulation depends on the level of vertical mix-
 327 ing (Wunsch & Ferrari, 2004) and in this configuration, that leads to the establishment
 328 of the southern hemisphere cell.

329 Compared to the cold climate state (Figure 5), the effects get more pronounced for
 330 the warm climate state (Figure 6) as already discussed in Section 3.2 for the effects of
 331 tidal heating alone.

332 4 Discussion

333 To help resolve the FYSP through tidal heating, the tidal heating rate would be
 334 required to contribute significantly to Earth’s energy balance. Based on global numbers,
 335 Archean tidal heating is generally considered to be too low to counteract the low solar
 336 input (Feulner, 2012), as even geothermal heat flux is greater by one order of magnitude.
 337 Although Heller et al. (2021) argue that tidal heating rates may be underestimated, they
 338 also conclude that tidal heating helped to maintain liquid surface water for the first 220
 339 Myr of Earth’s existence at most, and hence is most important during the Hadean rather
 340 than the Archean.

341 Our spatially-resolved simulations of tidal dissipation and its impact on climate con-
 342 firm that the tidal heat itself does not contribute to a measurable increase in the sur-
 343 face energy budget. Instead, tidal heating induces local changes in ocean currents and
 344 thus sea-ice dynamics and meridional heat transport. These secondary effects then may
 345 lead to regional cooling or warming of the ocean surface and associated changes in sea-
 346 ice cover, which amplify the changes in temperature via the ice-albedo feedback. On the
 347 other hand, our results also indicate that a large ice extent makes the climate more ro-
 348 bust against impacts from tidal heating due to the insulating effect of sea-ice cover. Fur-
 349 thermore, the impact of tidal heating on the global climate on early Earth is negligible.

350 However, including the effect of tidal dissipation on vertical mixing in the ocean
 351 leads to more pronounced warming. Combined with the heating from the higher geother-
 352 mal heat flux on early Earth, tides can thus contribute to warming the climate under
 353 the faint young Sun.

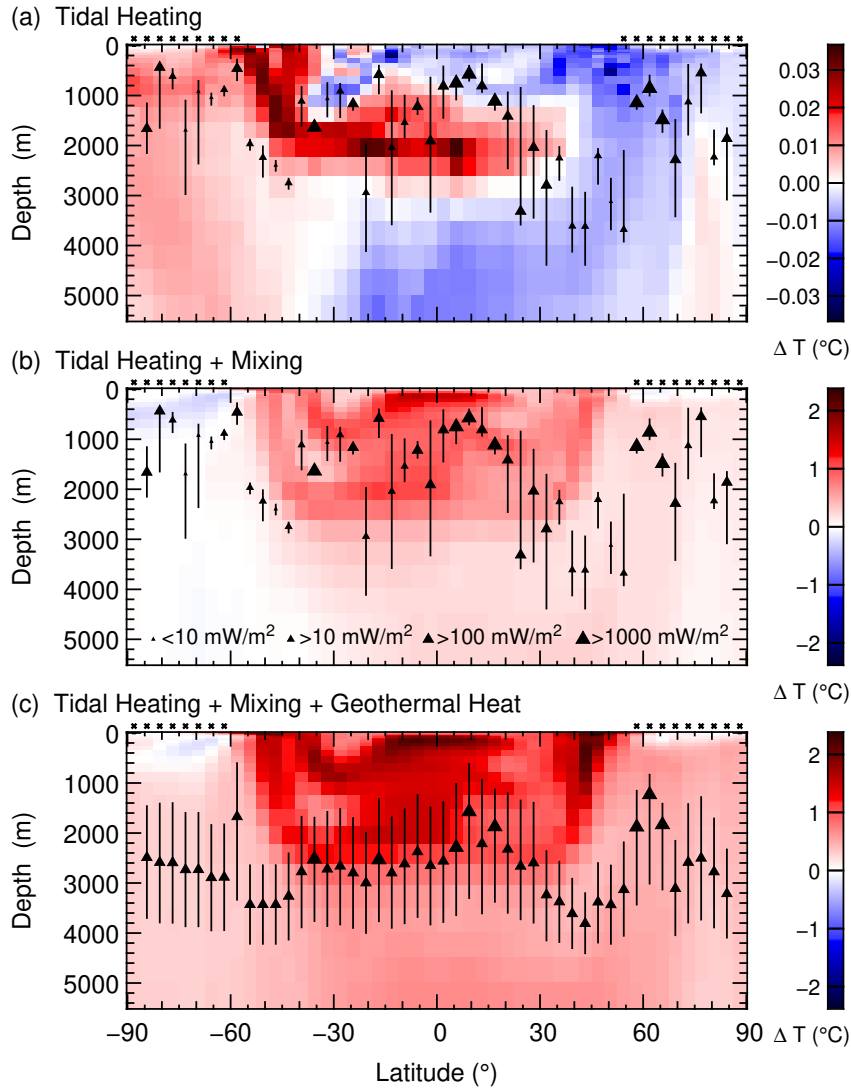


Figure 7. Depth-latitude section of potential temperature changes compared to the control simulation for a cold climate state and (a) tidal heating, (b) tidal heating plus mixing, and (c) tidal heating plus mixing plus geothermal heat flux (corresponding to the results shown in Figure 5). Note the much smaller temperature changes for just tidal heating in panel (a). Asterisks at the ocean surface indicate areas of at least 50% annual-mean sea-ice cover. The filled triangles in panels (a) and (b) indicate the second quartile of the depth distribution of tidal heating, with the size of the symbol scaled according to the magnitude of maximum heating. The vertical lines indicate the first and third quartiles, respectively. The corresponding combined energy input from tidal heating and geothermal heat is indicated in a similar manner in panel (c).

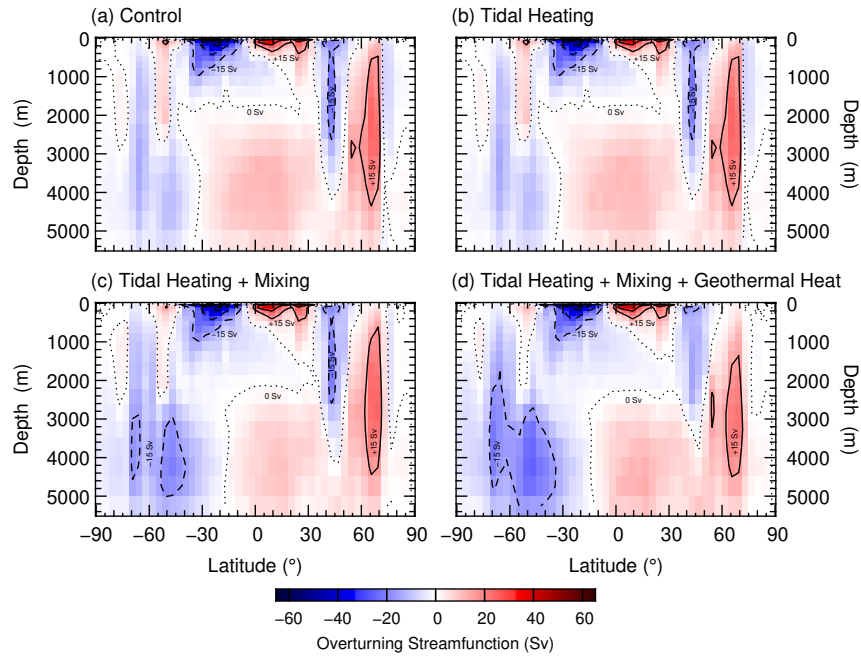


Figure 8. Global overturning streamfunction for a cold climate state with 12h rotation rate and (a) the control simulation, (b) tidal heating only, (c) tidal heating plus mixing, and (d) tidal heating, mixing, and geothermal heat flow (the simulations shown in Figures 5 and 7). Colours indicate the strength of the streamfunction. Contours are drawn in intervals of 15 Sv with negative values shown as dashed lines, the zero contour as dotted line, and positive values as solid lines.

354 Our approach of using a state-of-the-art tidal model and a coupled climate model
 355 to investigate the effects of tidal heating on early Earth’s climate spatially resolved can
 356 certainly be considered an improvement compared to simple global assessments. Nev-
 357 ertheless, our study is just a first step towards a more complete assessment of the influ-
 358 ence of tides on early Earth’s climate, with a number of questions still to be investigated.

359 First, one key factor determining tidal dissipation is the distribution of landmasses,
 360 which is unknown for early Earth. The continental configuration used in this study is
 361 randomly generated due to the lack of knowledge about Hadean and Archean Earth. As
 362 the landmasses strongly influence both the magnitude of tidal heating and its potential
 363 impact on meridional currents, the results of our study allow an assessment only for this
 364 particular continental configuration. Systematic ensemble investigations of different ran-
 365 dom continental configurations may find that there are scenarios in which lunar tides have
 366 a stronger influence on Earth’s climate compared to the configuration investigated above,
 367 considering that tidal dissipation can vary by three orders of magnitude for different land-
 368 ocean distributions (Blackledge et al., 2020) and that continental configuration can also
 369 significantly affect the snowball bifurcation point (Eberhard et al., 2023).

370 Second, the tides are not implemented dynamically, but the tidal dissipation fields
 371 are used to provide an additional heat source at the bottom of the ocean in the tidal heat-
 372 ing runs and to drive vertical mixing in the mixing runs. The change in the ocean tem-
 373 perature structure and overturning stream function as tidally driven mixing is implemented
 374 (Figures 7–8) show that using physically sound vertical mixing rates for the time period
 375 under consideration is necessary; present day mixing rates are poor proxy for past rates.

376 Third, despite the fact that the tidal heating and mixing are computed using a tidal
 377 model with day lengths of 12, 18 and 24 hours, our coupled climate model only simulates
 378 the climate dynamics of a present 24 hour length of day. Hence, any consequences of a
 379 faster rotation (e.g. the narrowing or appearance of additional atmospheric circulation
 380 cells) are not considered. Earlier work has shown that the snowball bifurcation is intri-
 381 cately linked to the large-scale circulation patterns in the atmosphere (Feulner et al., 2023).
 382 In this context it is important to note that there is still a large uncertainty in the evo-
 383 lution of Earth’s day length which translates also into a larger uncertainty in the rate
 384 of tidal heating at our chosen points in time.

385 Finally, tides within Earth’s mantle were dominant during the freezing of Earth’s
 386 surface in the first million years of the Hadean (Zahnle et al., 2007). After the mantle
 387 became solid, oceanic tides probably were the key driver for tidal heating (Blackledge
 388 et al., 2020), and hence our study focuses on ocean tides. More recent research (Daher
 389 et al., 2021) also investigated the impact of atmospheric tides which may have helped
 390 to stabilize Earth’s rotation, but the direct effect of these on the ocean would have been
 391 small. A more thorough investigation of tides in a magma ocean would be very inter-
 392 esting but is beyond our scope here.

393 5 Conclusions

394 In summary, our study uses spatially resolved maps of tidal dissipation from a state-
 395 of-the-art tidal model which represent more realistic tidal energy inputs compared to sim-
 396 ple exponential models or the CPL model by Heller et al. (2021) that assume a globally
 397 uniform tidal heating. By forcing a coupled climate model with this spatially-resolved
 398 tidal heating, tidal mixing, and geothermal heat flux our study makes a step further to-
 399 wards understanding the impacts of tides onto the climate on early Earth and contributes
 400 to assessing what role tides could have played in context of the FYSP.

401 Our results show that the global effect of tidal heating is insignificant but that tidal
 402 heating can affect sea-ice cover on local and regional scales and account for a substan-
 403 tial change in sea ice cover. In some scenarios the fraction of ice covered area of a grid

404 cell is altered by more than 20% due to the tidal heating. This impact is achieved by in-
 405 ducing changes in the ocean currents and thus in sea-ice dynamics as well as of heat trans-
 406 port towards the ice line. Tidal heating alone is thus certainly not the solution to the
 407 FYSP, as it does not provide enough energy. However, our results show that tidal heat-
 408 ing can have regional impacts. The fact that tidal heating acts primarily via altering oceanic
 409 currents underlines the importance of dynamical features when investigating tidal im-
 410 pacts.

411 Our study also shows that tidal mixing and geothermal heat flux are much more
 412 important than tidal heating alone. In particular the effects of tidal mixing should be
 413 included in future studies of deep-time paleoclimate states. With respect to the effect
 414 of tides on the climate on early Earth, future studies will have to investigate the effects
 415 of a shorter day length on the dynamics of the coupled Earth system under the faint young
 416 Sun and subject to stronger tidal forcing.

417 **Appendix A Global mean temperatures for all simulations**

418 **Appendix B Additional figures**

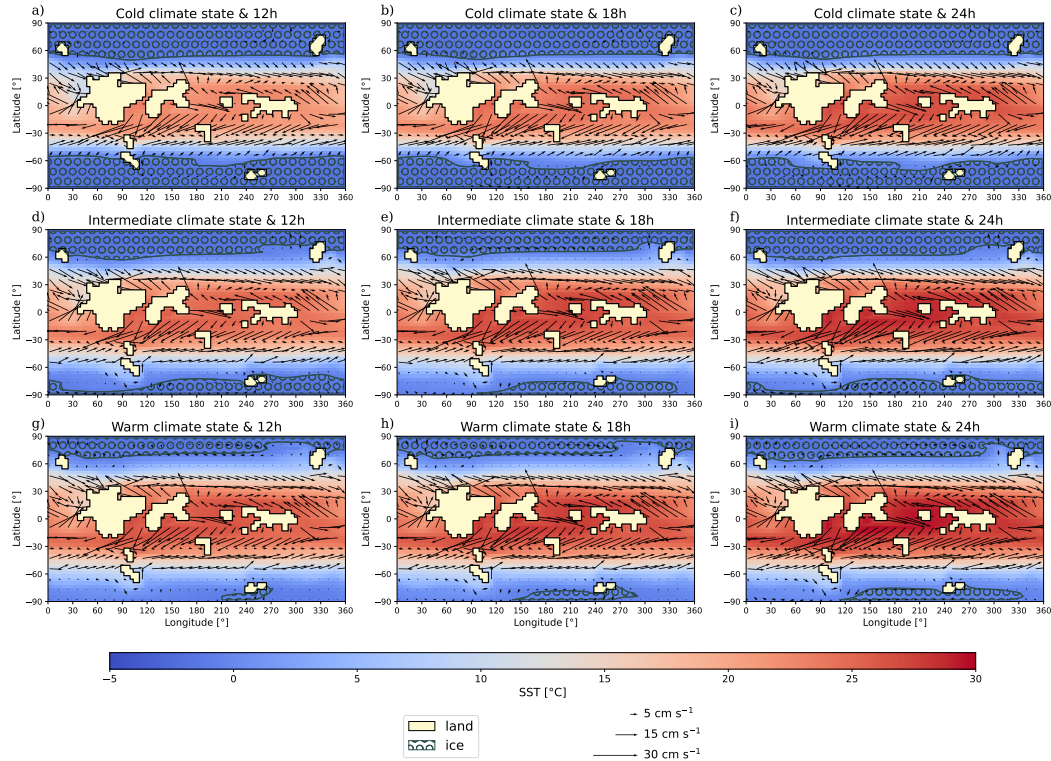


Figure B1. Control simulations. Absolute sea-surface temperatures (SSTs), surface velocities, and sea-ice cover (grid cells with annual-mean sea-ice fraction of at least 50%) for the nine control simulations without tides and geothermal heat flux.

419 **Acronyms**

420 **SST** Sea Surface Temperature

Table A1. Global and annual mean surface air temperatures (SATs) and sea-surface temperatures (SSTs) for all simulations. All values are computed over the last 500 years of each simulation.

S_0 [W/m ²]	CO ₂ [ppm]	Simulation	SAT [°C]	SST [°C]
1010	176000	Control	9.23	12.0
		Tidal heating	9.22	12.0
		Tidal heating + mixing	9.95	12.4
		Tidal heating + mixing + geothermal	11.0	13.1
	200000	Control	14.3	15.3
		Tidal heating	14.2	15.3
		Tidal heating + mixing	14.8	15.8
		Tidal heating + mixing + geothermal	15.0	16.0
	220000	Control	16.7	17.2
		Tidal heating	16.7	17.2
		Tidal heating + mixing	17.0	17.4
		Tidal heating + mixing + geothermal	17.2	17.6
1161	15000	Control	10.7	13.4
		Tidal heating	10.7	13.4
		Tidal heating + mixing	10.8	13.4
		Tidal heating + mixing + geothermal	10.9	13.5
	25000	Control	16.3	17.2
		Tidal heating	16.3	17.2
		Tidal heating + mixing	16.3	17.2
		Tidal heating + mixing + geothermal	16.5	17.3
	28000	Control	17.5	18.0
		Tidal heating	17.5	18.0
		Tidal heating + mixing	17.5	18.0
		Tidal heating + mixing + geothermal	17.6	18.1
1361	140	Control	11.8	14.8
		Tidal heating	11.8	14.8
		Tidal heating + mixing	11.9	14.8
		Tidal heating + mixing + geothermal	12.0	14.9
	277	Control	16.1	17.6
		Tidal heating	16.2	17.6
		Tidal heating + mixing	16.2	17.7
		Tidal heating + mixing + geothermal	16.3	17.7
	350	Control	17.7	18.7
		Tidal heating	17.7	18.7
		Tidal heating + mixing	18.0	18.9
		Tidal heating + mixing + geothermal	18.1	19.0

421 **CLIMBER** CLIMate-BiosphERe Model
422 **EMIC** Earth system Model of Intermediate Complexity
423 **FYSP** Faint Young Sun Problem
424 **GCM** General Circulation Model
425 **AOGCM** Atmospheric-Oceanic General Circulation Model

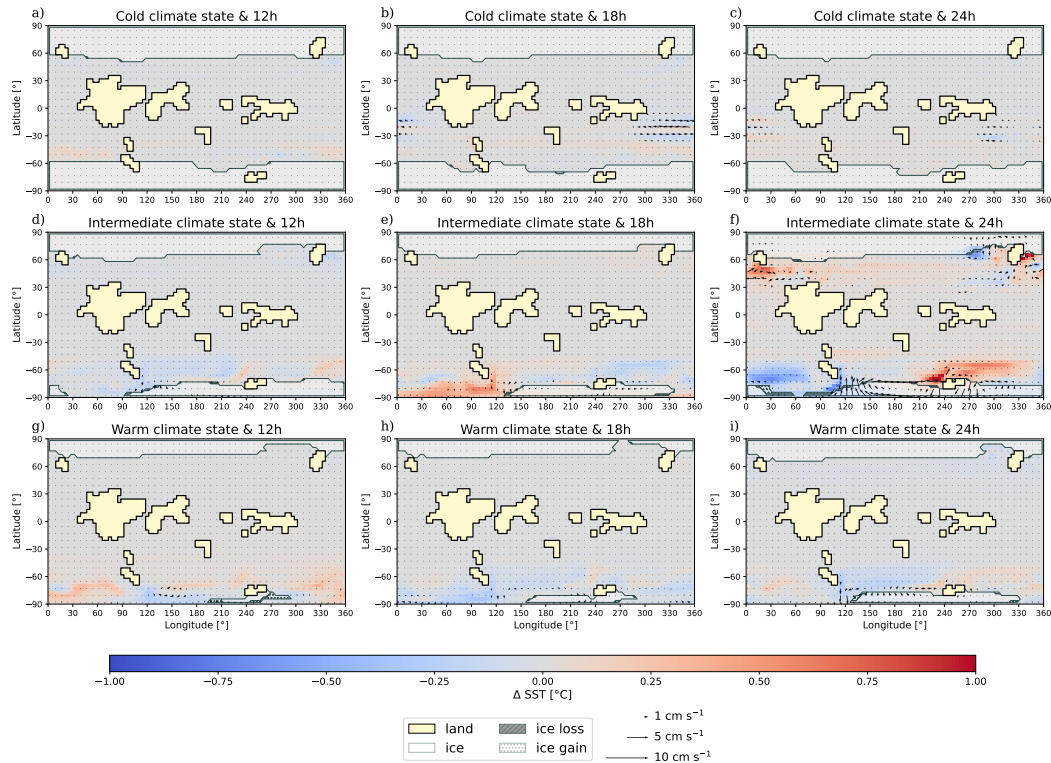


Figure B2. Simulations with tidal heating. Changes in sea-surface temperature, surface velocity, and sea-ice cover due to tidal heating for three different tidal scenarios with (a,d,g) 12 h, (b,e,h) 18 h, and (c,f,i) 24 h rotation rate and for (a,b,c) low, (d,e,f) intermediate, and (g,h,i) high CO₂ levels corresponding to cold, intermediate, and warm climate states, respectively. The blue and red colors correspond to changes in SST when introducing tidal heating. Yellow areas are land; semi-transparent white areas correspond to regions that are covered have at least 50% sea-ice fraction in the annual mean. Dotted and hatched areas represent regions of sea-ice loss or gain, respectively. Arrows indicate a change in ocean surface currents, with their length scaling with the change in speed. Figure 3 corresponds to the panels in the second row, Figure 4 to the ones in the first column.

426

Open Research Section

427

428

429

430

431

432

433

All model input and output files as well as the pre-processing and post-processing scripts used to generate model input and the figures in the paper are published with DOI 10.5880/PIK.2023.004 via the GFZ data portal. The DOI will be activated upon publication of the manuscript. The data is already available at <http://www.pik-potsdam.de/data/doi/10.5880/PIK.2023.004/> (preview URL). The source code for the model used in this study is archived at the Potsdam Institute for Climate Impact Research and is made available upon request.

434

Acknowledgments

435

436

437

The European Regional Development Fund (ERDF), the German Federal Ministry of Education and Research and the Land Brandenburg are gratefully acknowledged for supporting this project by providing resources on the high performance computer system

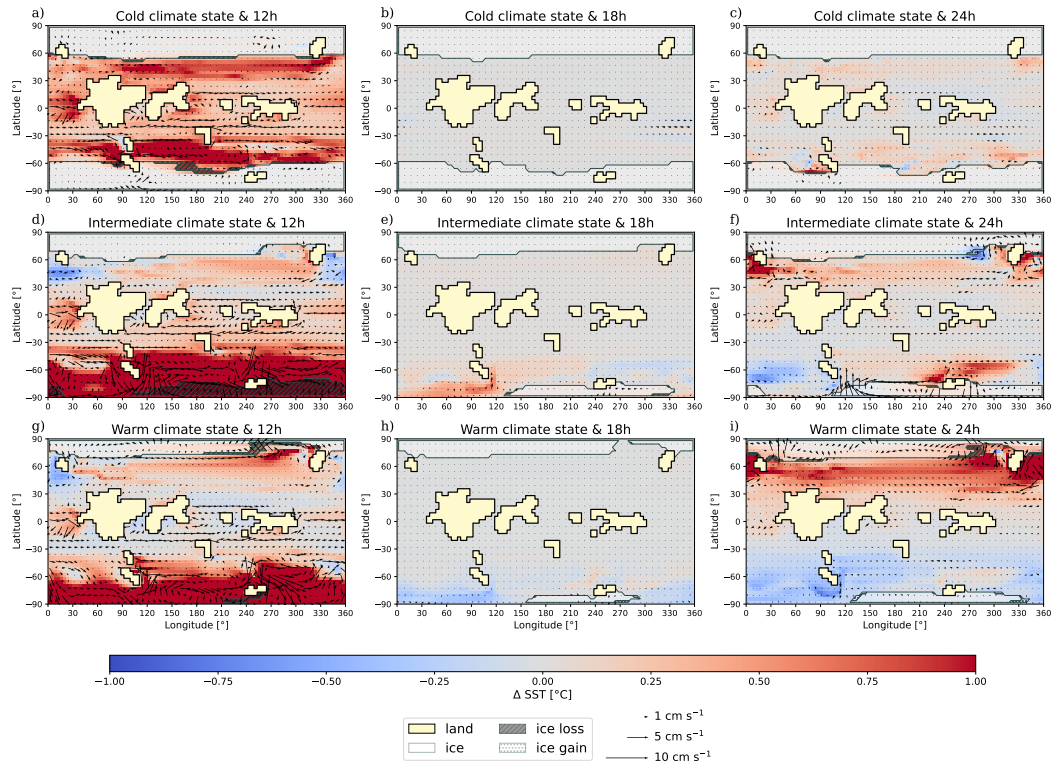


Figure B3. Simulations with tidal heating and mixing. Same as Figure B2 but for the simulations also including the effects of tidal mixing. Note that the mixing parameters for 18 hours daylength are the same as the default model parameters.

438 at the Potsdam Institute for Climate Impact Research. JAMG acknowledges funding from
 439 The Leverhulme trust (grant RPG-2021-091) and The Natural Environment Research
 440 Council (grant NE/S009566/1). The tidal model simulations were done on Supercom-
 441 puting Wales through Bangor University. The authors thank two anonymous reviewers
 442 and the editor, Matthew Huber, for their comments which helped improve the manuscript.

443 References

- 444 Balbus, S. A. (2014). Dynamical, biological and anthropic consequences of equal
 445 lunar and solar angular radii. *Proceedings of the Royal Society A: Mathematical,*
 446 *Physical and Engineering Sciences*, *470*(2168). (arXiv: 1406.0323) doi: 10
 447 .1098/rspa.2014.0263
 448 Barnes, R., Raymond, S. N., Jackson, B., & Greenberg, R. (2008). Tides and the
 449 evolution of planetary habitability. *Astrobiology*, *8*, 557-568. doi: 10.1089/ast
 450 .2007.0204
 451 Bills, B. G., & Ray, R. D. (1999). Lunar orbital evolution: A synthesis of recent re-
 452 sults. *Geophysical Research Letters*, *26*, 3045-3048.
 453 Blackledge, B., Green, M., Barnes, R., & Way, M. (2020). Tides on Other Earths:
 454 Implications for Exoplanet and Palaeo-Tidal Simulations. *Geophysical Research*
 455 *Letters*, *47*, e2019GL085746. doi: 10.1029/2019GL085746
 456 Byrne, H. M., Green, J. A., Balbus, S. A., & Ahlberg, P. E. (2020). Tides: A
 457 key environmental driver of osteichthyan evolution and the fish-tetrapod

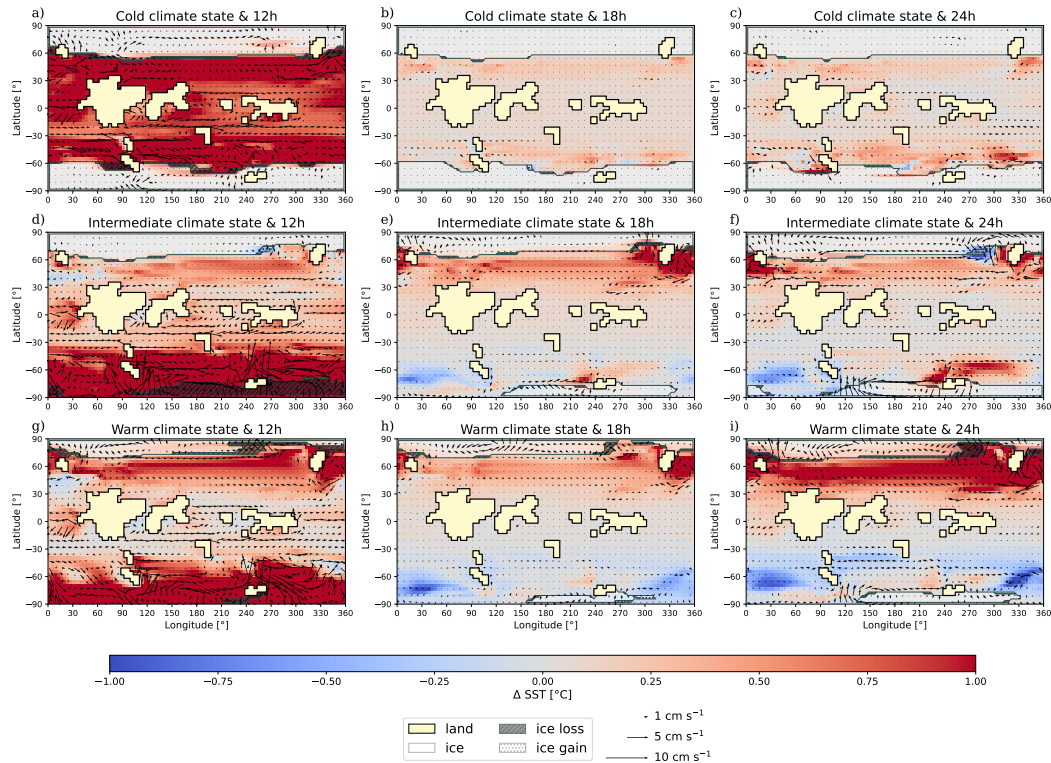


Figure B4. Simulations with tidal heating, mixing, and geothermal heat flux. Same as Figure B3 but for the simulations also including the effects of geothermal heat flux.

- 458 transition? *Proceedings of the Royal Society A: Mathematical, Physical and*
 459 *Engineering Sciences*, 476(2242). doi: 10.1098/rspa.2020.0355
- 460 Cawood, P. A., Chowdhury, P., Mulder, J. A., Hawkesworth, C. J., Capitanio, F. A.,
 461 Gunawardana, P. M., & Nebel, O. (2022). Secular evolution of continents
 462 and the earth system. *Reviews of Geophysics*, 60(4), e2022RG000789. doi:
 463 10.1029/2022RG000789
- 464 Daher, H., Arbic, B. K., Williams, J. G., Ansong, J. K., Boggs, D. H., Müller, M.,
 465 ... Huber, M. (2021). Long-Term Earth-Moon Evolution With High-Level
 466 Orbit and Ocean Tide Models. *Journal of Geophysical Research: Planets*,
 467 126(12), e2021JE006875. doi: 10.1029/2021JE006875
- 468 Eberhard, J., Bevan, O. E., Feulner, G., Petri, S., van Hunen, J., & Baldini, J. U. L.
 469 (2023). Sensitivity of neoproterozoic snowball-earth inceptions to continen-
 470 tal configuration, orbital geometry, and volcanism. *Climate of the Past*, 19,
 471 2203–2235. doi: 10.5194/cp-19-2203-2023
- 472 Egbert, G. D., Bills, B. G., & Ray, R. D. (2004). Numerical modeling of the global
 473 semidiurnal tide in the present day and in the last glacial maximum. *Journal*
 474 *of Geophysical Research*, 109, C03003, doi: 10.1029/2003JC001973.
- 475 Egbert, G. D., & Ray, R. D. (2001). Estimates of M2 tidal energy dissipation from
 476 Topex/Poseidon altimeter data. *Journal of Geophysical Research*, 106, 22475-
 477 22502.
- 478 Eulendorf, T., & Heubeck, C. (2023). Constraints on Moon's Orbit 3.2 Billion Years
 479 Ago From Tidal Bundle Data. *Journal of Geophysical Research (Planets)*,
 480 128(1), e2022JE007466. doi: 10.1029/2022JE007466

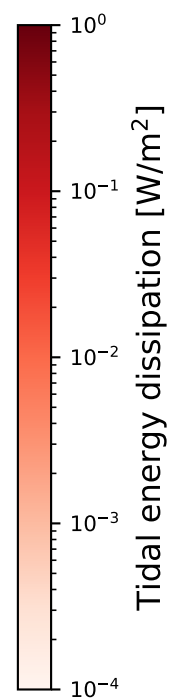
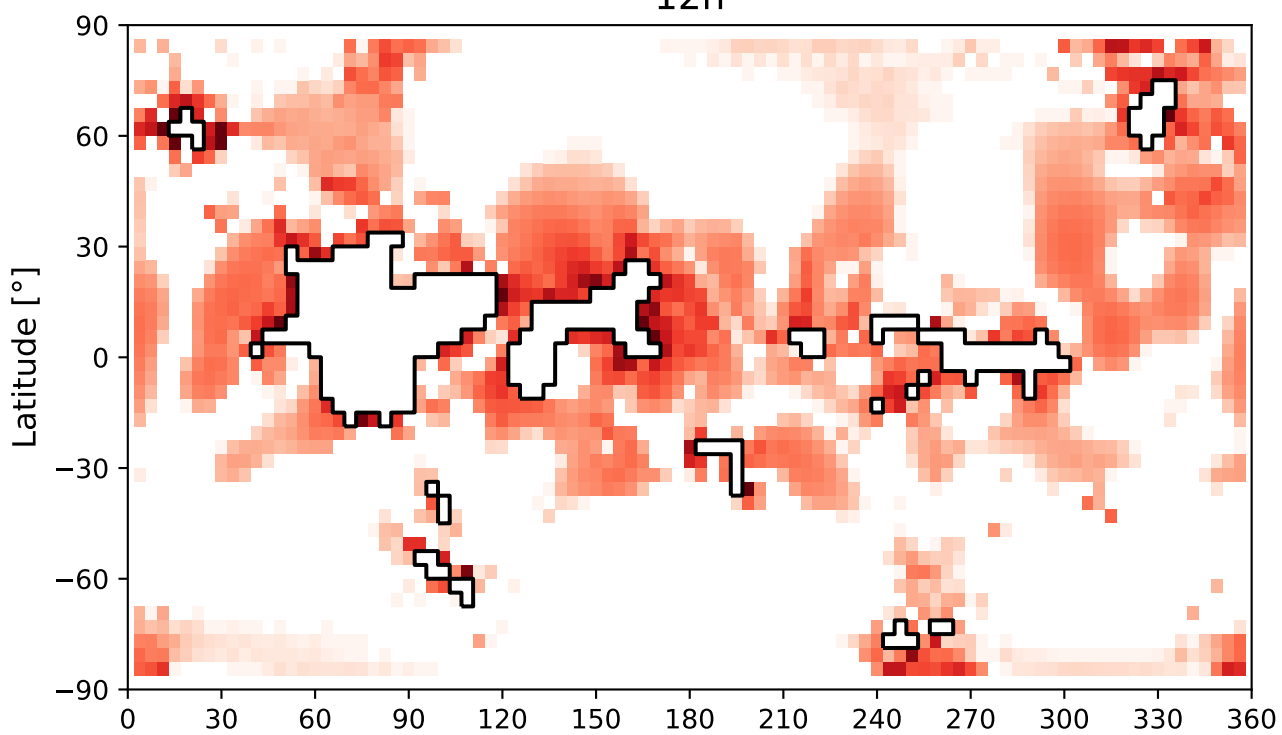
- 481 Farhat, M., Auclair-Desrotour, P., Boué, G., & Laskar, J. (2022). The resonant
482 tidal evolution of the Earth-Moon distance. *Astronomy & Astrophysics*, *665*,
483 L1. doi: 10.1051/0004-6361/202243445
- 484 Feulner, G. (2012). The faint young sun problem. *Rev. Geophys.*, *50*, RG2006. doi:
485 10.1029/2011RG000375
- 486 Feulner, G. (2017). Formation of most of our coal brought Earth close to global
487 glaciation. *Proc. Natl. Acad. Sci.*, *114*(43), 11333-11337. doi: 10.1073/pnas
488 .1712062114
- 489 Feulner, G., Bukenberger, M., & Petri, S. (2023). Tracing the Snowball bi-
490 furcation of aquaplanets through time reveals a fundamental shift in
491 critical-state dynamics. *Earth System Dynamics*, *14*(3), 533-547. doi:
492 10.5194/esd-14-533-2023
- 493 Feulner, G., Hallmann, C., & Kienert, H. (2015). Snowball cooling after algal rise.
494 *Nature Geosci.*, *8*, 659-662. doi: 10.1038/ngeo2523
- 495 Feulner, G., & Kienert, H. (2014). Climate simulations of Neoproterozoic snow-
496 ball Earth events: Similar critical carbon dioxide levels for the Sturtian
497 and Marinoan glaciations. *Earth Planet. Sc. Lett.*, *404*, 200-205. doi:
498 10.1016/j.epsl.2014.08.001
- 499 Fichet, T., & Morales Maqueda, M. A. (1997). Sensitivity of a global sea ice model
500 to the treatment of ice thermodynamics and dynamics. *J. Geophys. Res. -*
501 *Oceans*, *102*(C6), 12609-12646. doi: 10.1029/97JC00480
- 502 Green, J. A. M. (2010). Ocean tides and resonance. *Ocean Dynamics*, *60*. doi: 10
503 .1007/s10236-010-0331-1
- 504 Green, J. A. M., Davies, H. S., Duarte, J. C., Creveling, J. R., & Scotese, C. (2020).
505 Weak tides during Cryogenian glaciations. *Nature Communications*, *11*(1),
506 6227. doi: 10.1038/s41467-020-20008-3
- 507 Green, J. A. M., & Duarte, J. C. e. (2022). *A journey through tides* (J. A. M. Green
508 & J. C. Duarte, Eds.). Elsevier.
- 509 Green, J. A. M., & Huber, M. (2013). Tidal dissipation in the early Eocene
510 and implications for ocean mixing. *Geophysical Research Letters*, *40*,
511 doi:10.1002/grl.50510.
- 512 Green, J. A. M., Huber, M., Waltham, D., Buzan, J., & Wells, M. (2017). Ex-
513 plicitly modelled deep-time tidal dissipation and its implication for Lu-
514 nar history. *Earth and Planetary Science Letters*, *461*, 46-53. doi:
515 10.1016/j.epsl.2016.12.038
- 516 Green, J. A. M., Molloy, J. L., Davies, H. S., & Duarte, J. C. (2018). Is there a tec-
517 tonically driven supertidal cycle? *Geophysical Research Letters*, *45*, 3568-3576.
518 doi: 10.1002/2017GL076695
- 519 Green, J. A. M., & Nycander, J. (2013). A comparison of internal wave drag param-
520 eterizations for tidal models. *Journal of Physical Oceanography*, *43*, 104-119.
- 521 Hawkesworth, C. J., Cawood, P. A., & Dhuime, B. (2020). The evolution of the con-
522 tinental crust and the onset of plate tectonics. *Frontiers in Earth Science*, *8*.
523 doi: 10.3389/feart.2020.00326
- 524 Heller, R., Duda, J.-P., Winkler, M., Reitner, J., & Gizon, L. (2021). Habit-
525 ability of the early Earth: liquid water under a faint young Sun facilitated
526 by strong tidal heating due to a closer Moon. *PalZ*, *95*, 563-575. doi:
527 10.1007/s12542-021-00582-7
- 528 Hofmann, M., & Morales Maqueda, M. A. (2006). Performance of a second-order
529 moments advection scheme in an Ocean General Circulation Model. *J. Geo-*
530 *phys. Res.*, *111*(C5), C05006. doi: 10.1029/2005JC003279
- 531 Jermyn, A. S., Bauer, E. B., Schwab, J., Farmer, R., Ball, W. H., Bellinger, E. P.,
532 ... Timmes, F. X. (2023). Modules for Experiments in Stellar Astrophysics
533 (MESA): Time-dependent Convection, Energy Conservation, Automatic Dif-
534 ferentiation, and Infrastructure. *Astrophys. J. (Supp.)*, *265*(1), 15. doi:
535 10.3847/1538-4365/acae8d

- 536 Kienert, H., Feulner, G., & Petoukhov, V. (2012). Faint young Sun problem more
537 severe due to ice-albedo feedback and higher rotation rate of the early Earth.
538 *Geophys. Res. Lett.*, *39*, L23710. doi: 10.1029/2012GL054381
- 539 Kienert, H., Feulner, G., & Petoukhov, V. (2013). Albedo and heat transport in 3-D
540 model simulations of the early Archean climate. *Clim. Past*, *9*, 1841-1862. doi:
541 10.5194/cp-9-1841-2013
- 542 Klatt, J. M., Chennu, A., Arbic, B. K., Biddanda, B. A., & Dick, G. J. (2021). Pos-
543 sible link between Earth's rotation rate and oxygenation. *Nature Geoscience*,
544 *14*, 564–570. doi: 10.1038/s41561-021-00784-3
- 545 MacDonald, G. J. F. (1964, August). Tidal friction. *Reviews of Geo-*
546 *physics*, *2*(3), 467. Retrieved 2018-09-04, from [http://doi.wiley.com/
547 10.1029/RG002i003p00467](http://doi.wiley.com/10.1029/RG002i003p00467) (Publisher: Wiley-Blackwell) doi: 10.1029/
548 RG002i003p00467
- 549 Montoya, M., Griesel, A., Levermann, A., Mignot, J., Hofmann, M., Ganopolski, A.,
550 & Rahmstorf, S. (2005). The earth system model of intermediate complexity
551 CLIMBER-3 α . Part I: description and performance for present-day conditions.
552 *Climate Dynamics*, *25*(2), 237–263. doi: 10.1007/s00382-005-0044-1
- 553 Pacanowski, R. C., & Griffies, S. M. (1999). *The MOM-3 manual* (Tech. Rep.
554 No. 4). Princeton, NJ, USA: NOAA/Geophysical Fluid Dynamics Lab-
555 oratory. Retrieved from [https://mom-ocean.github.io/assets/pdfs/
556 MOM3_manual.pdf](https://mom-ocean.github.io/assets/pdfs/MOM3_manual.pdf)
- 557 Petoukhov, V., Ganopolski, A., Brovkin, V., Claussen, M., Eliseev, A., Kubatzki, C.,
558 & Rahmstorf, S. (2000). CLIMBER-2: a climate system model of intermediate
559 complexity. Part I: model description and performance for present climate.
560 *Clim. Dyn.*, *16*(1), 1–17. doi: 10.1007/pl00007919
- 561 Pollack, H. N., Hurter, S. J., & Johnson, J. R. (1993, August). Heat flow from the
562 earth's interior - Analysis of the global data set. *Reviews of Geophysics*, *31*(3),
563 267-280. doi: 10.1029/93RG01249
- 564 Sawada, H. (2020). Estimation of secular change in the size of continents for un-
565 derstanding early crustal development. *Frontiers in Earth Science*, *8*. doi: 10
566 .3389/feart.2020.541094
- 567 Schmittner, A., Green, J. A. M., & Wilmes, S.-B. (2015). Glacial ocean overturning
568 intensified by tidal mixing in a global circulation model. *Geophysical Research*
569 *Letters*, *42*, doi:10.1002/2015GL0635610.
- 570 Sharples, J., Tweddle, J., Green, J., Palmer, M., Kim, Y.-N., Hickman, A., ...
571 Krivtsov, V. (2007). Spring-neap modulation of internal tide mixing and
572 vertical nitrate fluxes at a shelf edge in summer. *Limnology and Oceanography*,
573 *52*(5). doi: 10.4319/lo.2007.52.5.1735
- 574 Tuerena, R., Williams, R., Mahaffey, C., Vic, C., Green, J., Naveira-Garabato, A.,
575 ... Sharples, J. (2019). Internal Tides Drive Nutrient Fluxes Into the Deep
576 Chlorophyll Maximum Over Mid-ocean Ridges. *Global Biogeochemical Cycles*,
577 *33*(8). doi: 10.1029/2019GB006214
- 578 Turcotte, D. L., & Schubert, G. (2002). *Geodynamics*. Cambridge University Press.
- 579 Wilmes, S., Green, J. A. M., & Schmittner, A. (2021). Enhanced vertical mixing in
580 the glacial ocean inferred from sedimentary carbon isotopes. *Nature Communi-*
581 *cations Earth and Environment*, *2*(166).
- 582 Wunsch, C., & Ferrari, R. (2004). Vertical mixing, energy, and the general cir-
583 culation of the oceans. *Annual Review of Fluid Mechanics*, *36*, 281-314, doi:10.
584 1146/annurev.fluid.36.050802.122121.
- 585 Yang, J., Boué, G., Fabrycky, D. C., & Abbot, D. S. (2014). Strong dependence of
586 the inner edge of the habitable zone on planetary rotation rate. *Astrophysical*
587 *Journal Letters*, *787*(1). (arXiv: 1404.4992) doi: 10.1088/2041-8205/787/1/
588 L2
- 589 Zahnle, K., Arndt, N., Cockell, C., Halliday, A., Nisbet, E., Selsis, F., & Sleep, N. H.
590 (2007). Emergence of a Habitable Planet. *Space Science Reviews*, *129*(1),

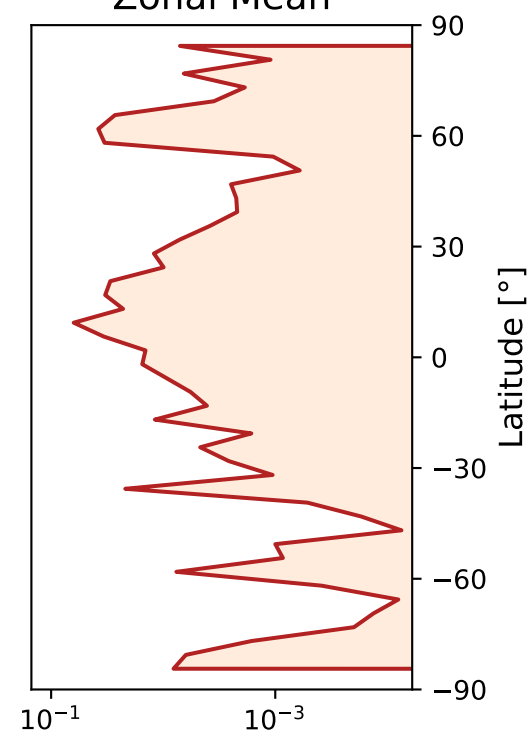
591 35-78. doi: 10.1007/s11214-007-9225-z
592 Zaron, E. D., & Egbert, G. D. (2006). Estimating open-ocean barotropic tidal
593 dissipation: The Hawaiian Ridge. *Journal of Physical Oceanography*, 36,
594 1019-1035.

Figure 1.

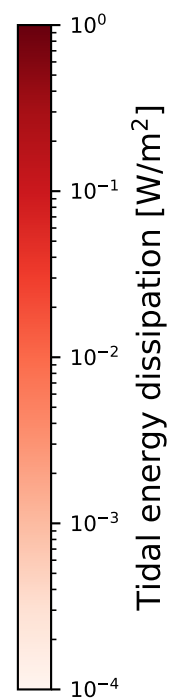
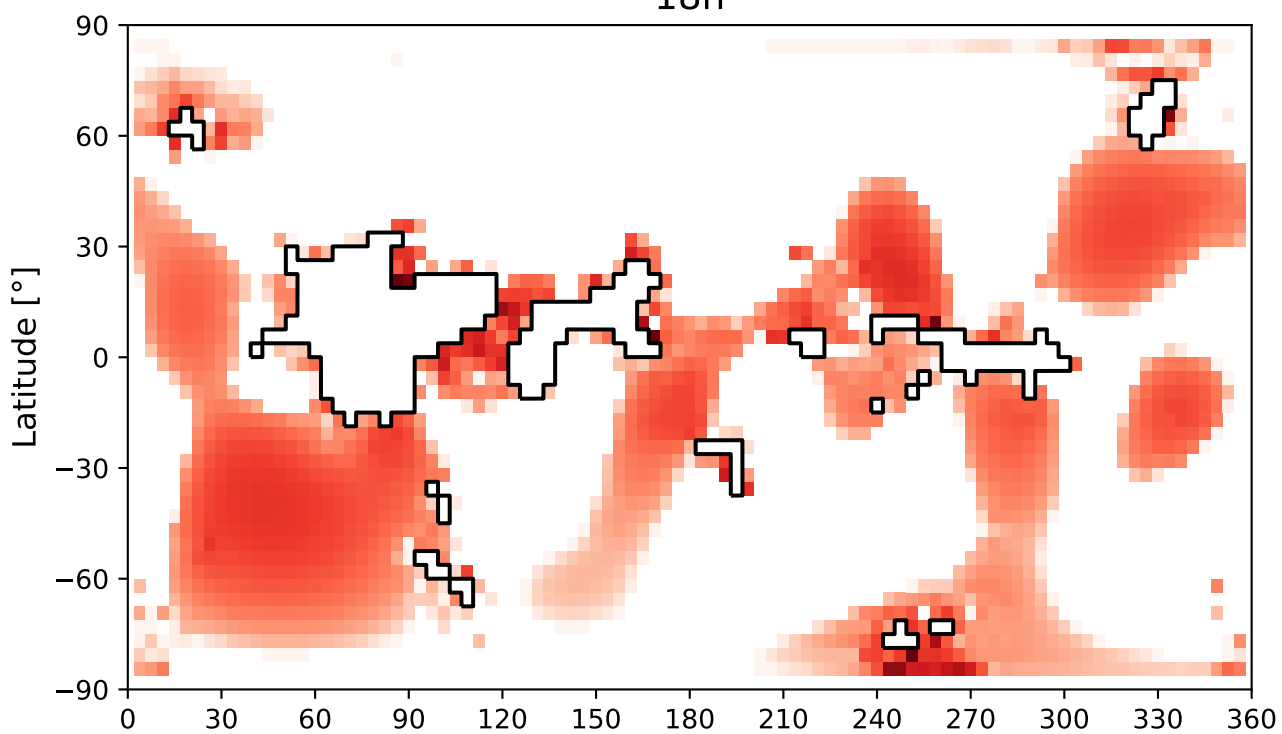
12h



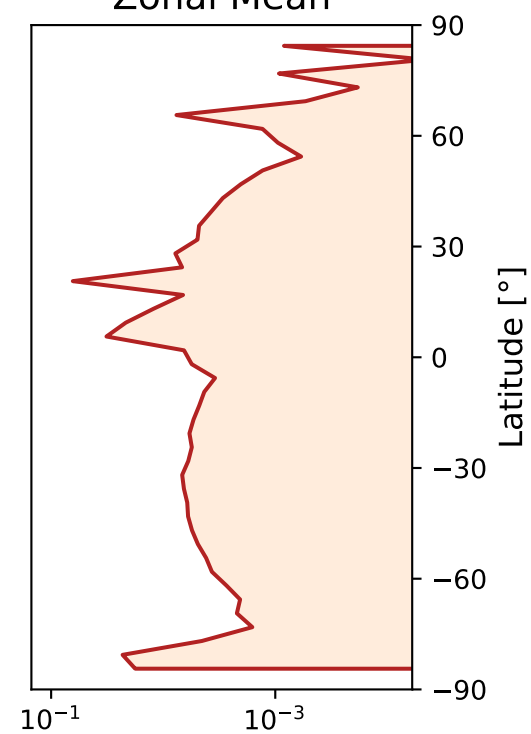
Zonal Mean



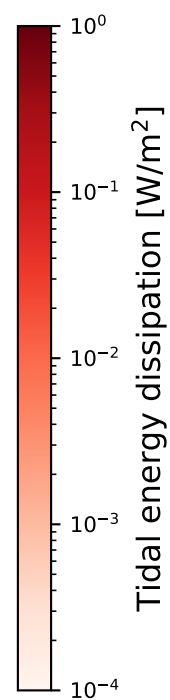
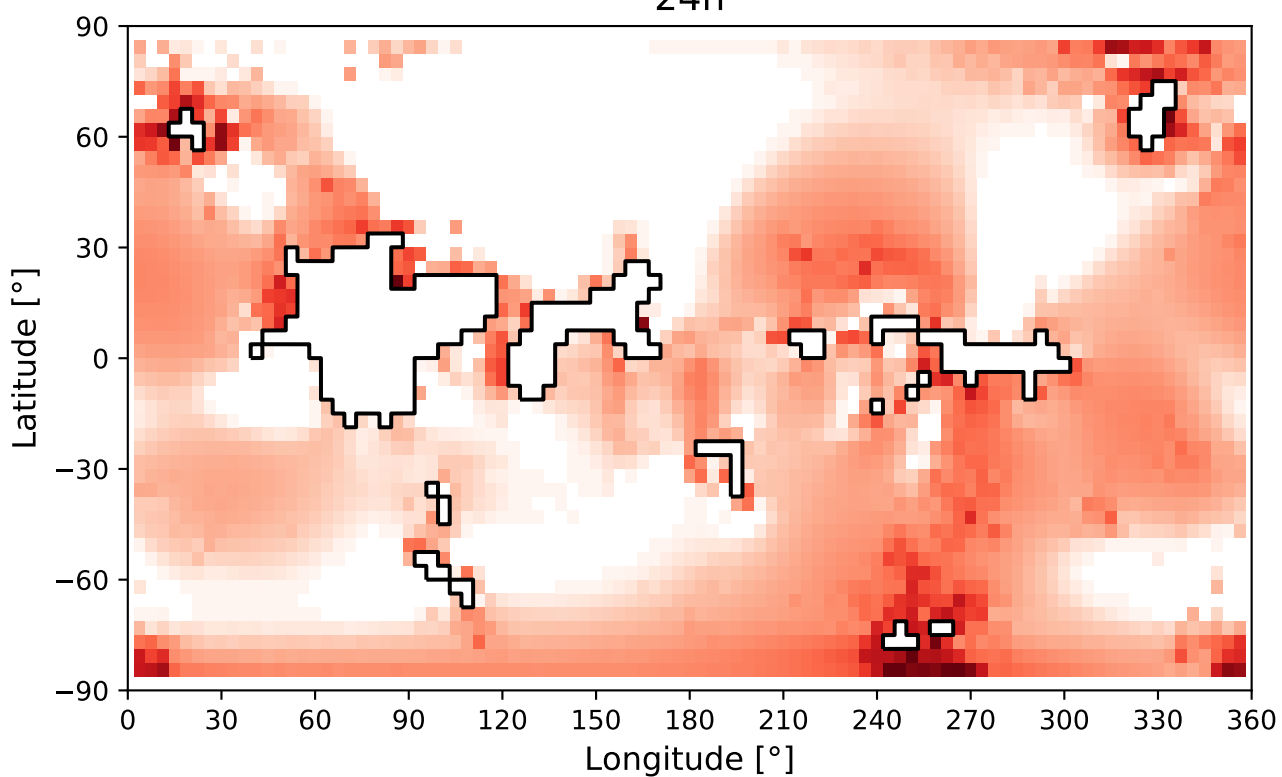
18h



Zonal Mean



24h



Zonal Mean

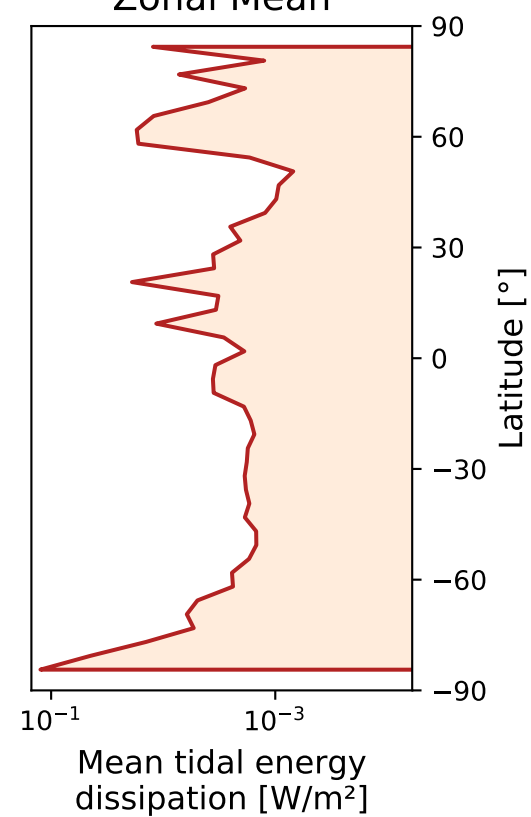


Figure 2.

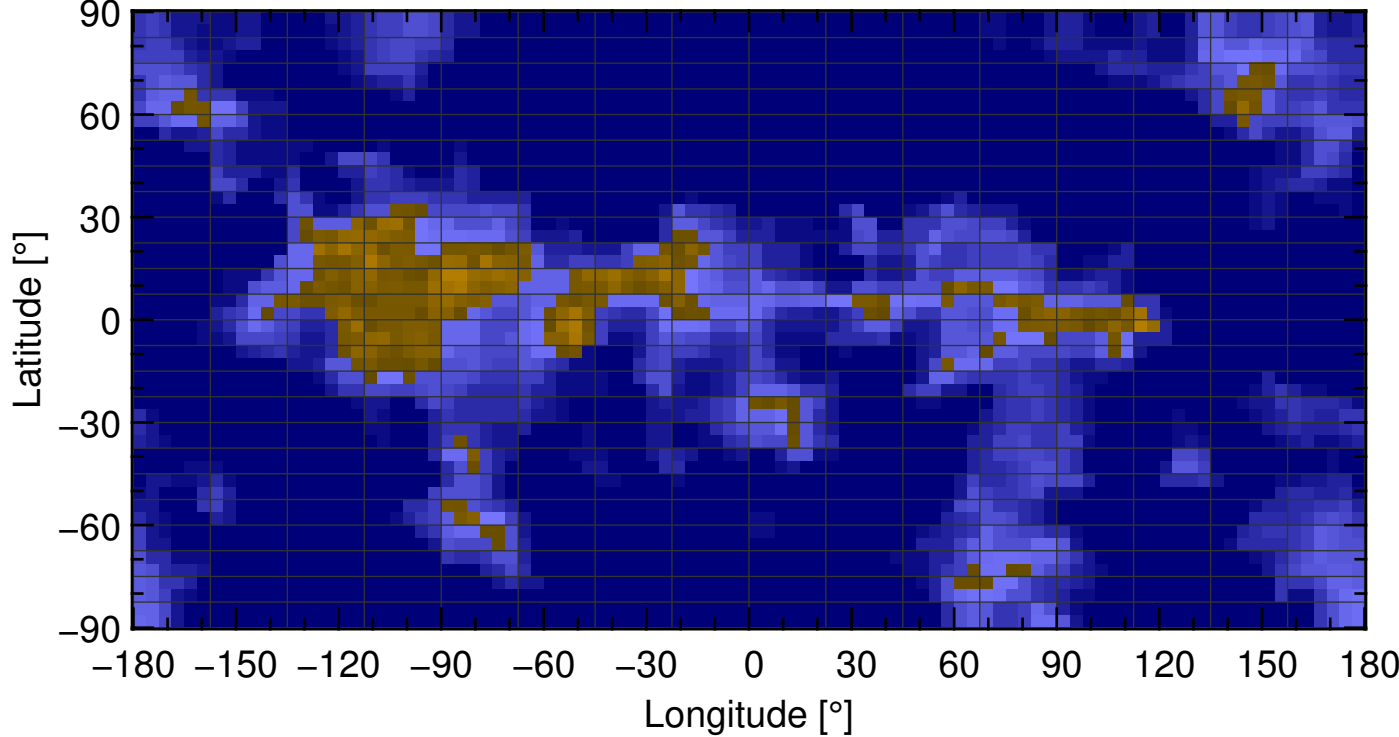


Figure 3.

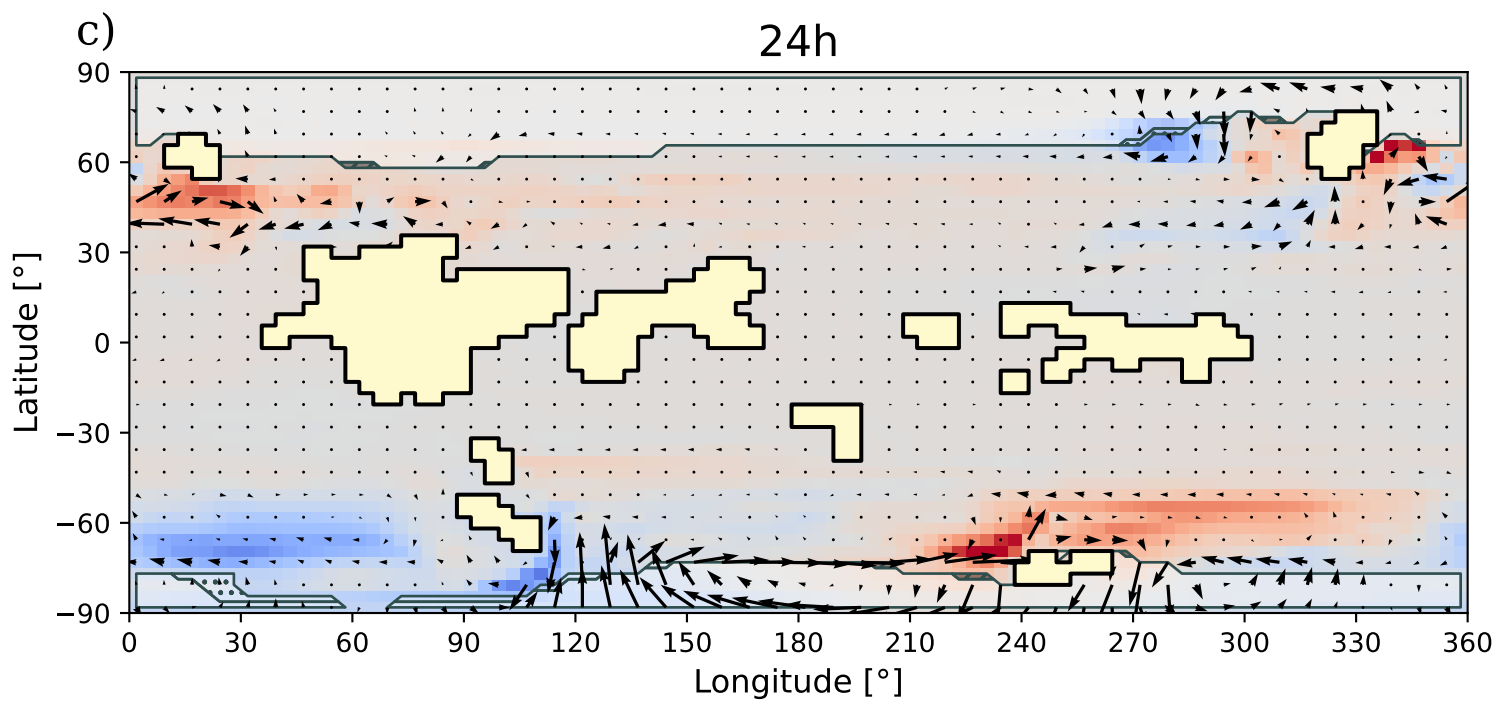
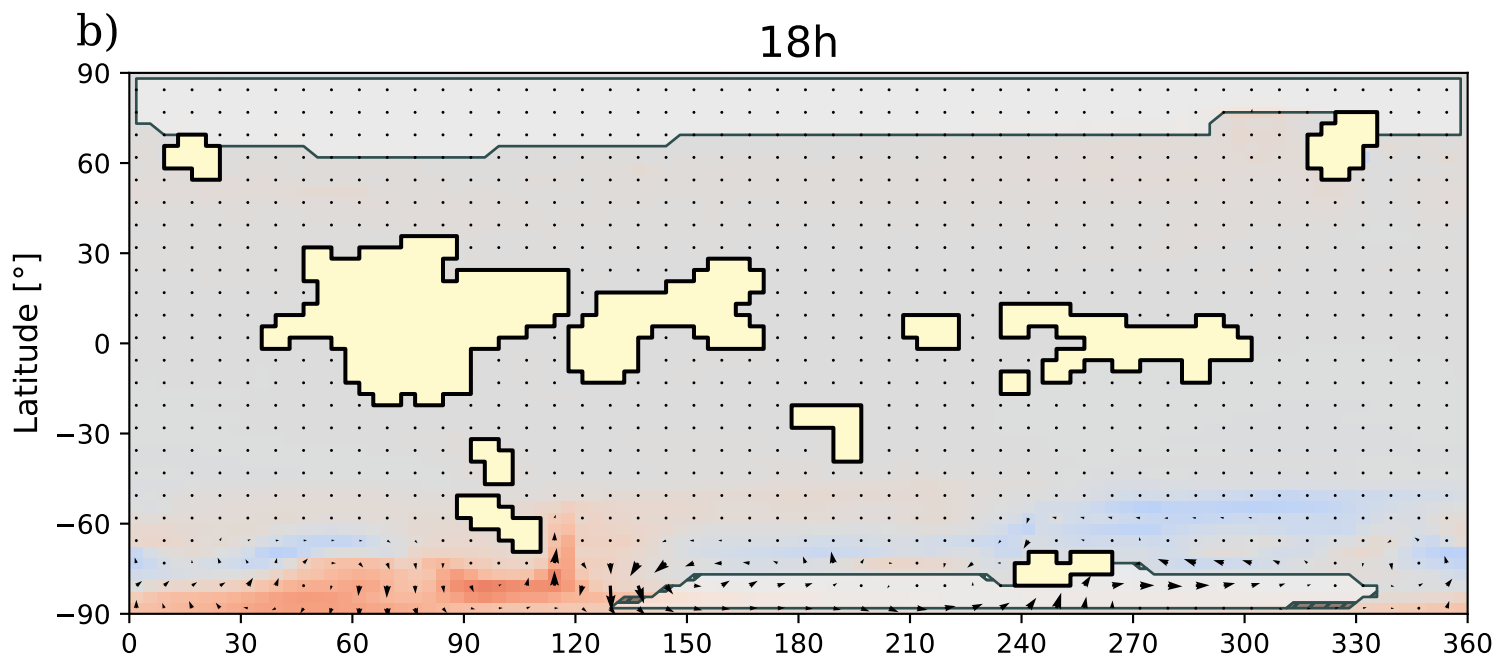
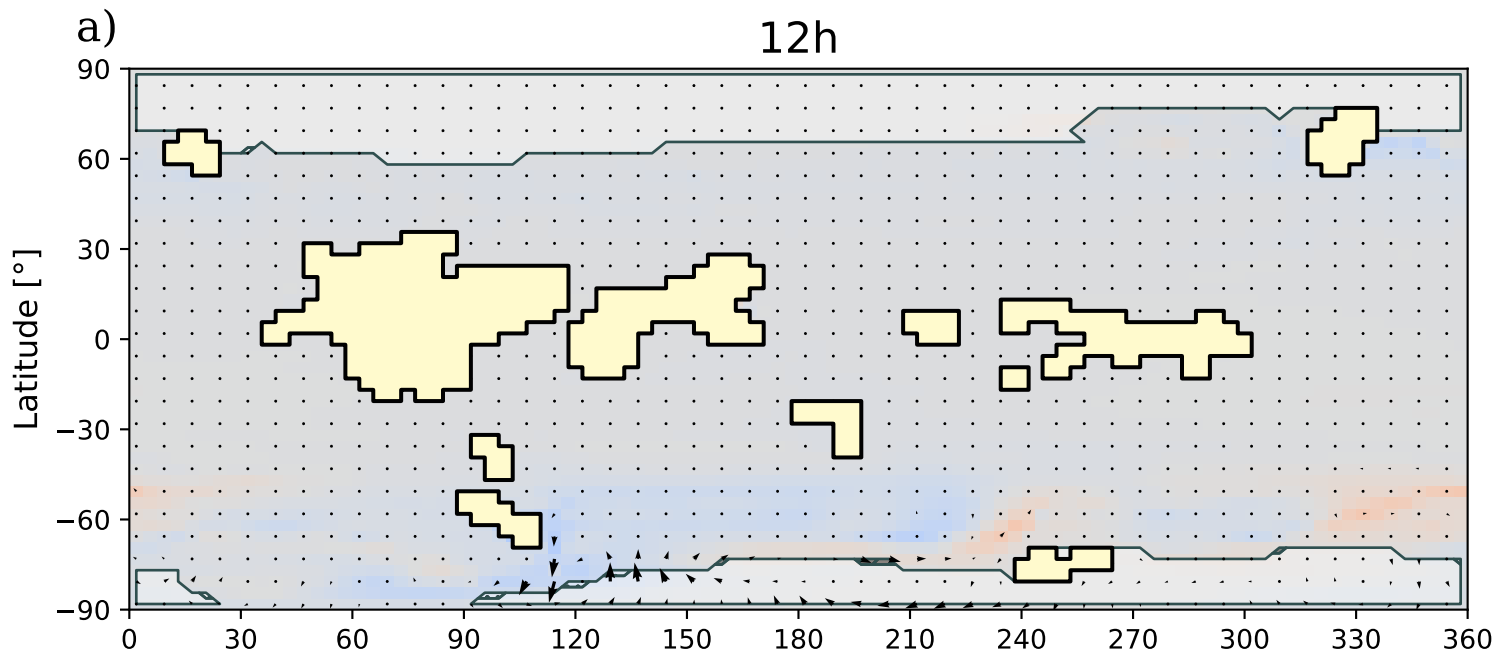
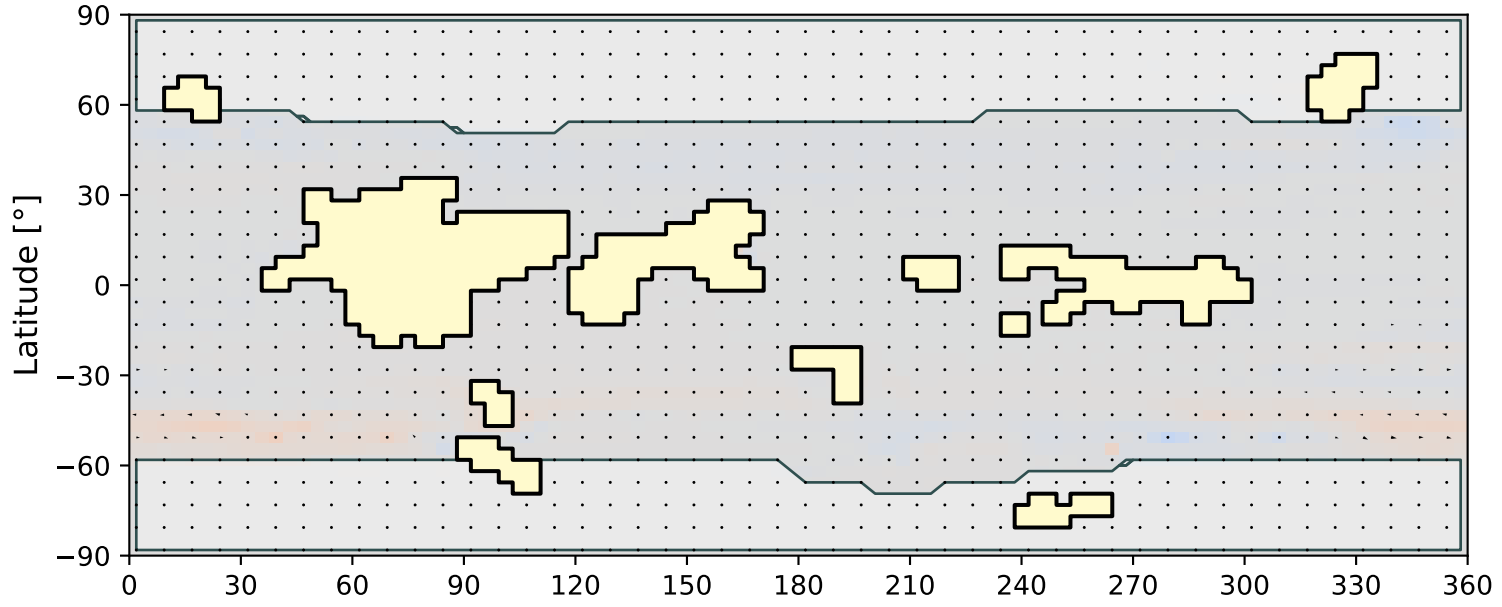
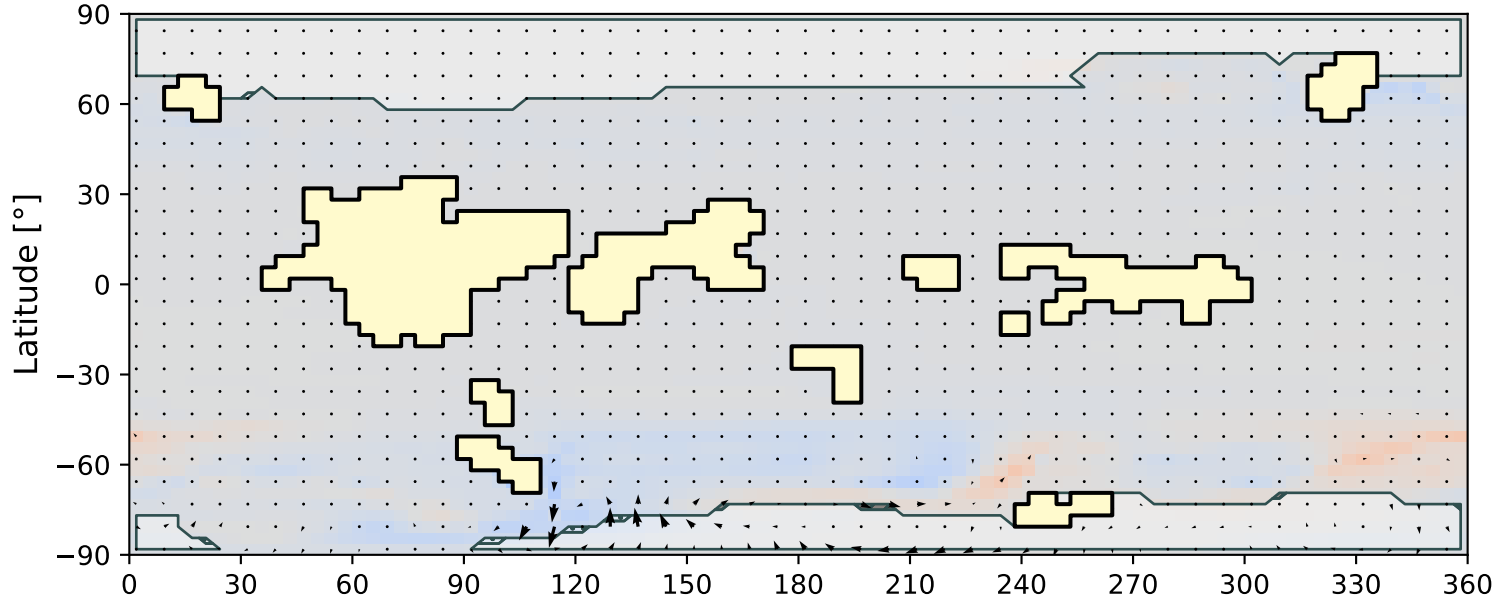


Figure 4.

a) Cold climate state



b) Intermediate climate state



c) Warm climate state

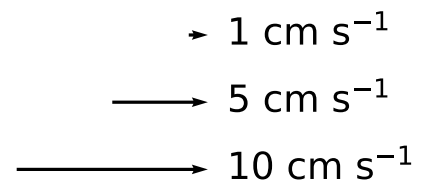
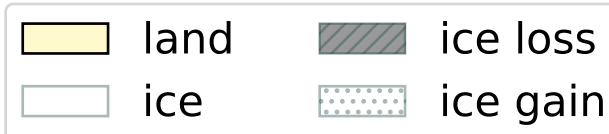
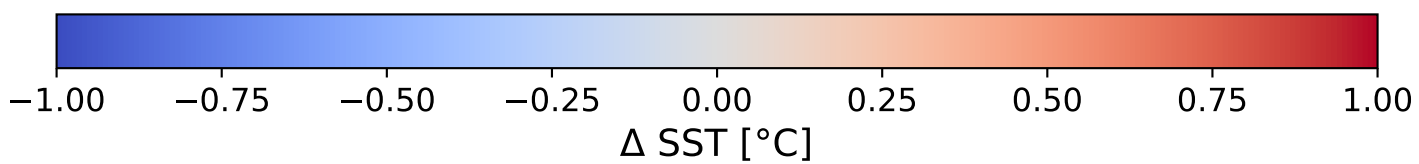
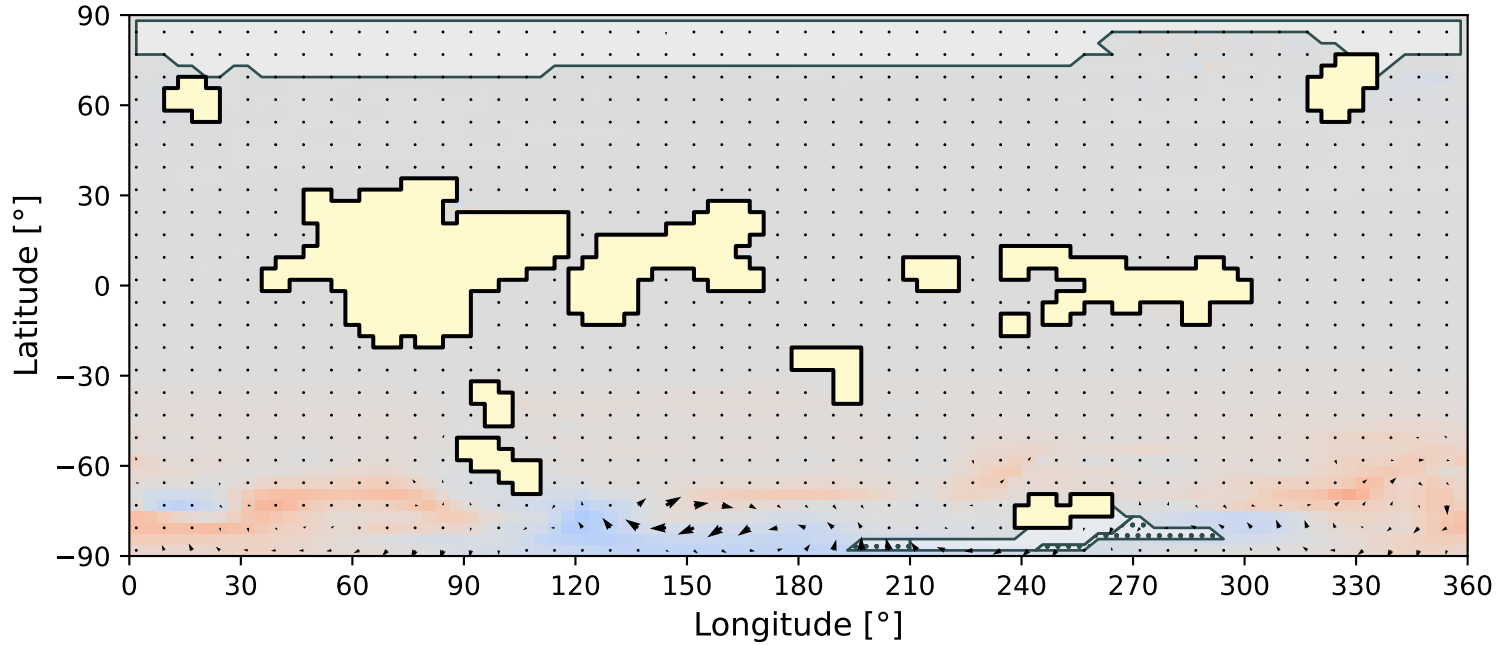


Figure 5.

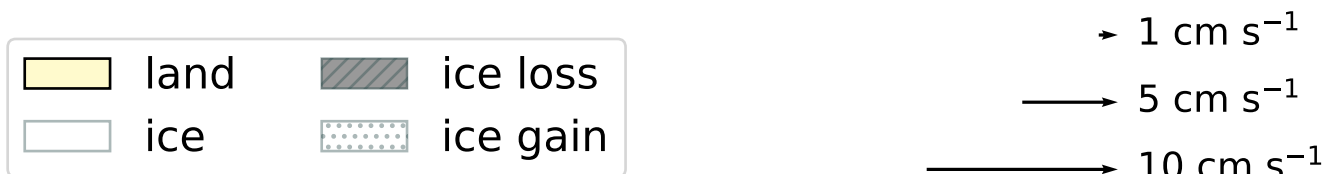
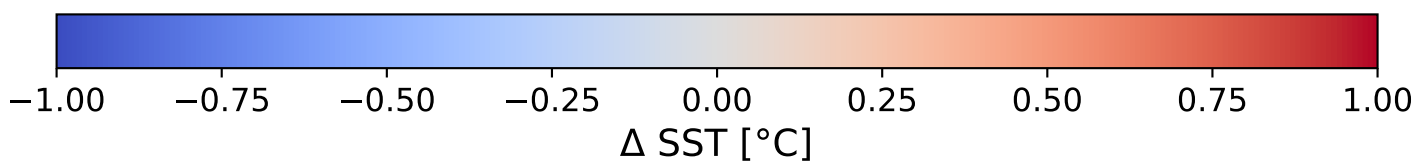
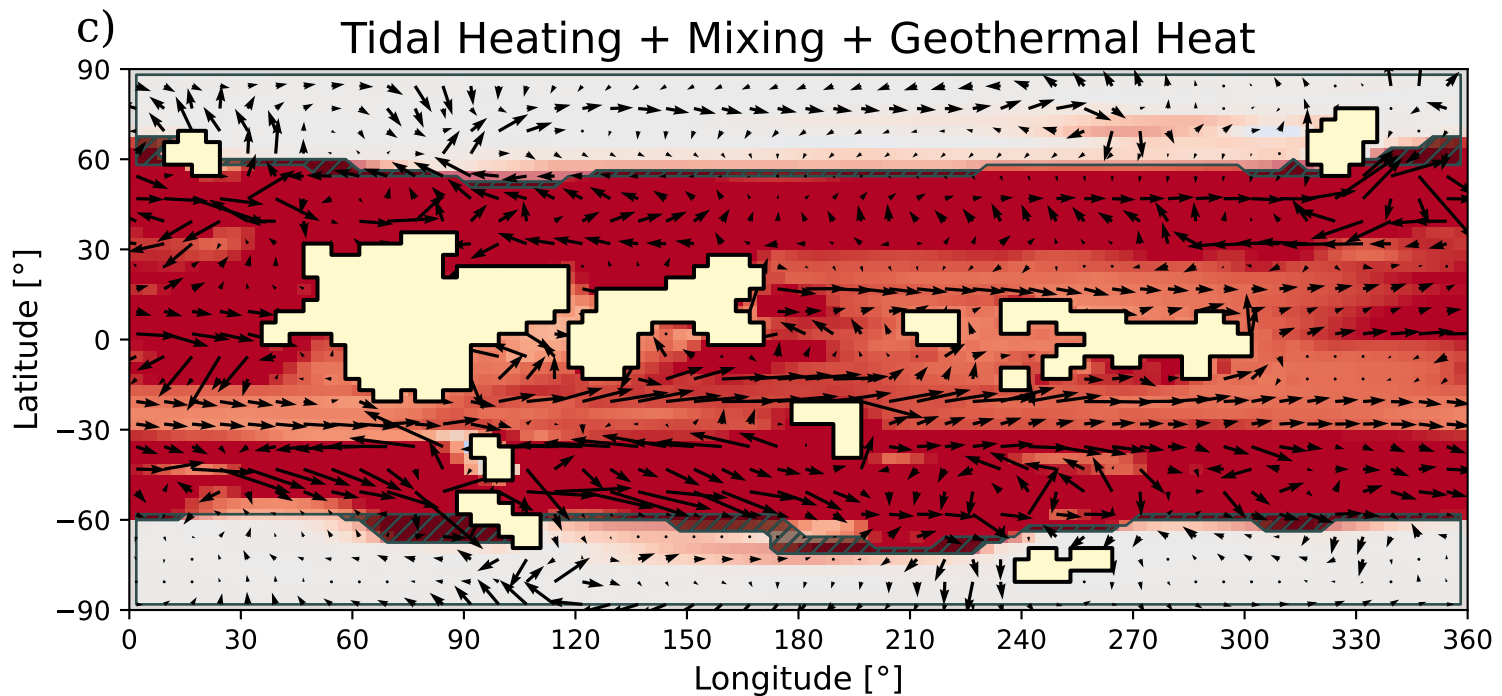
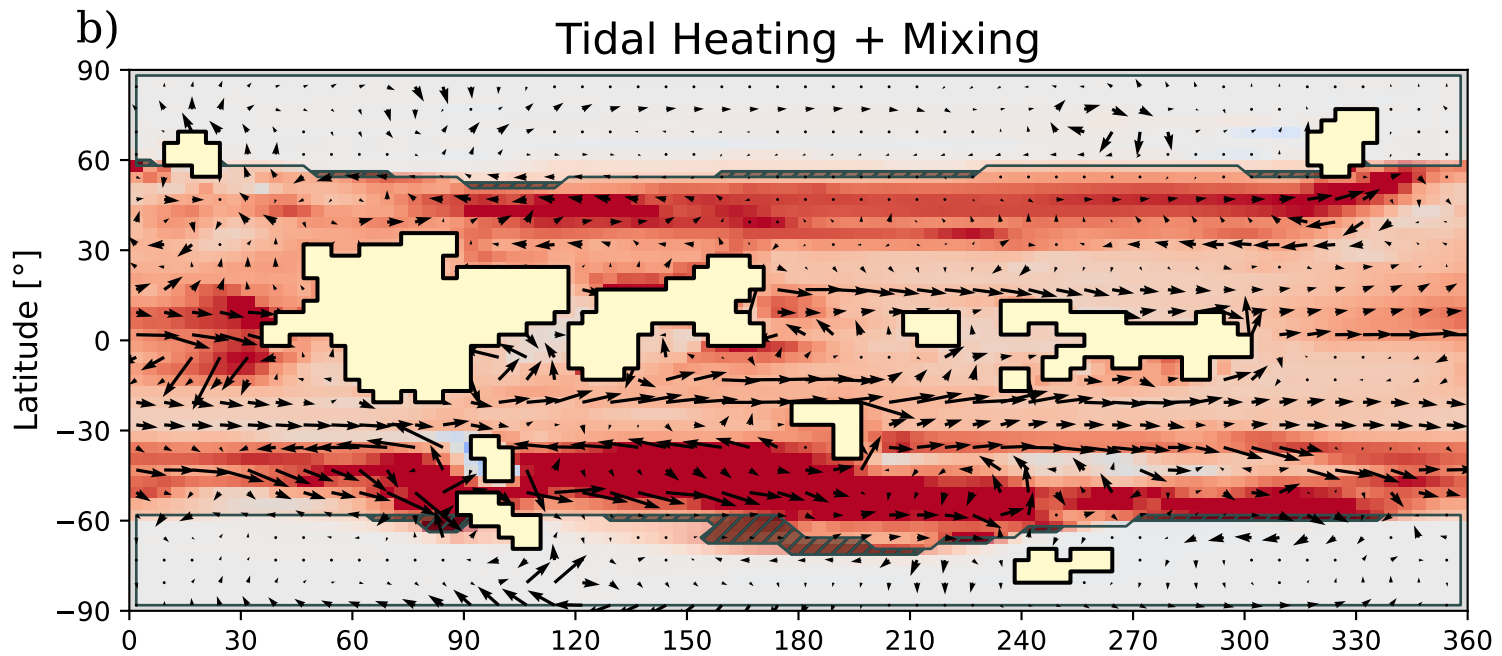
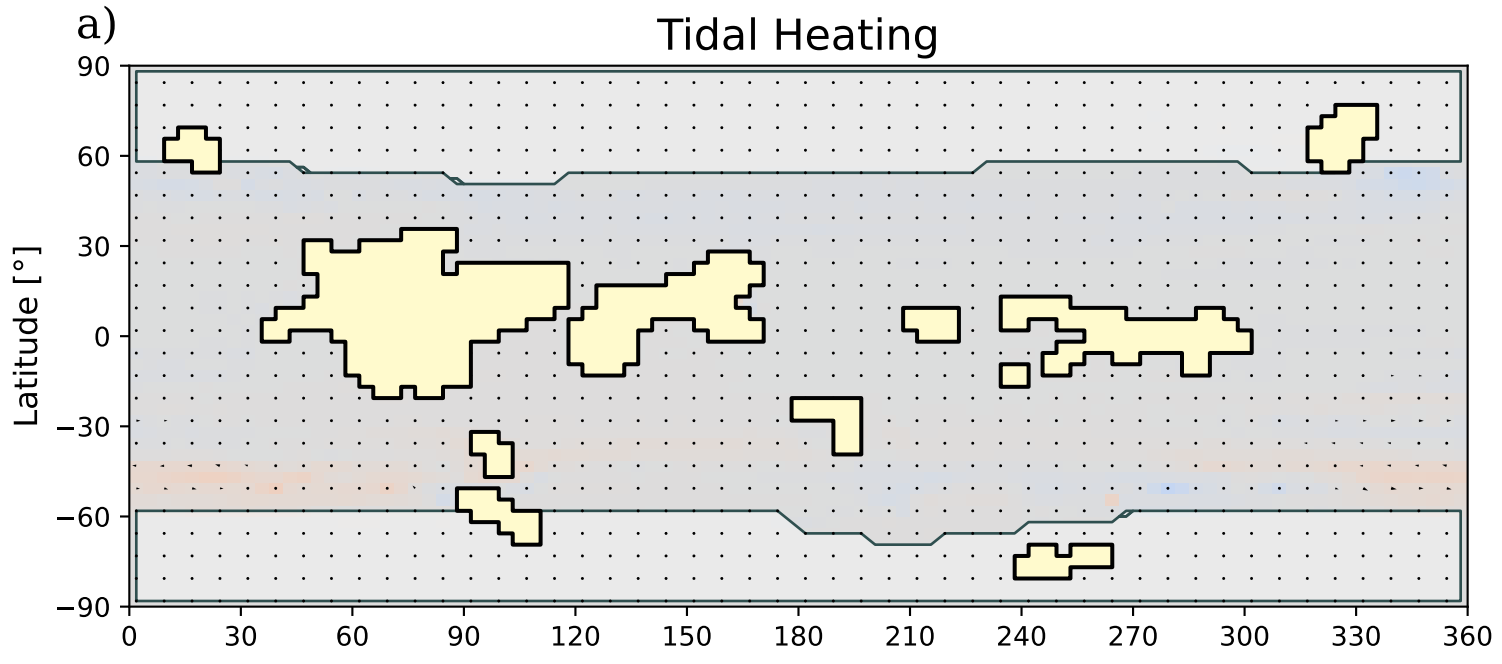


Figure 6.

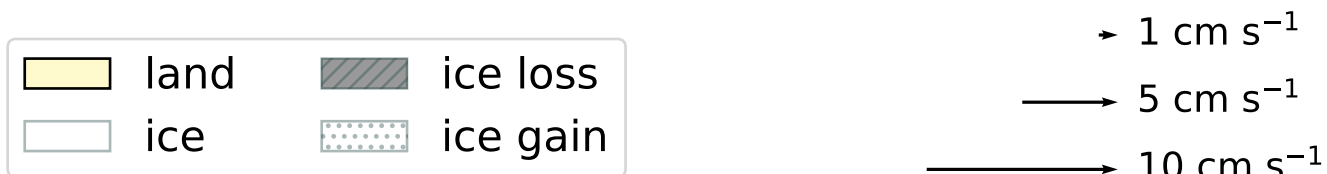
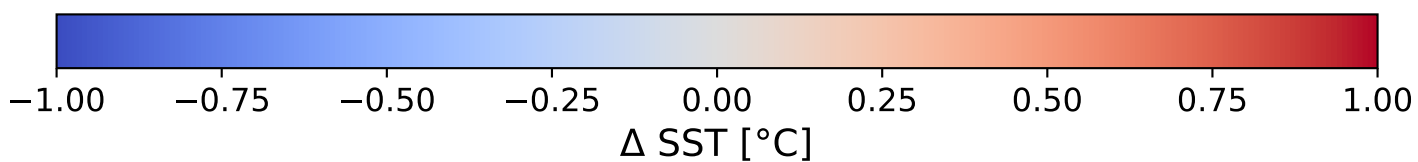
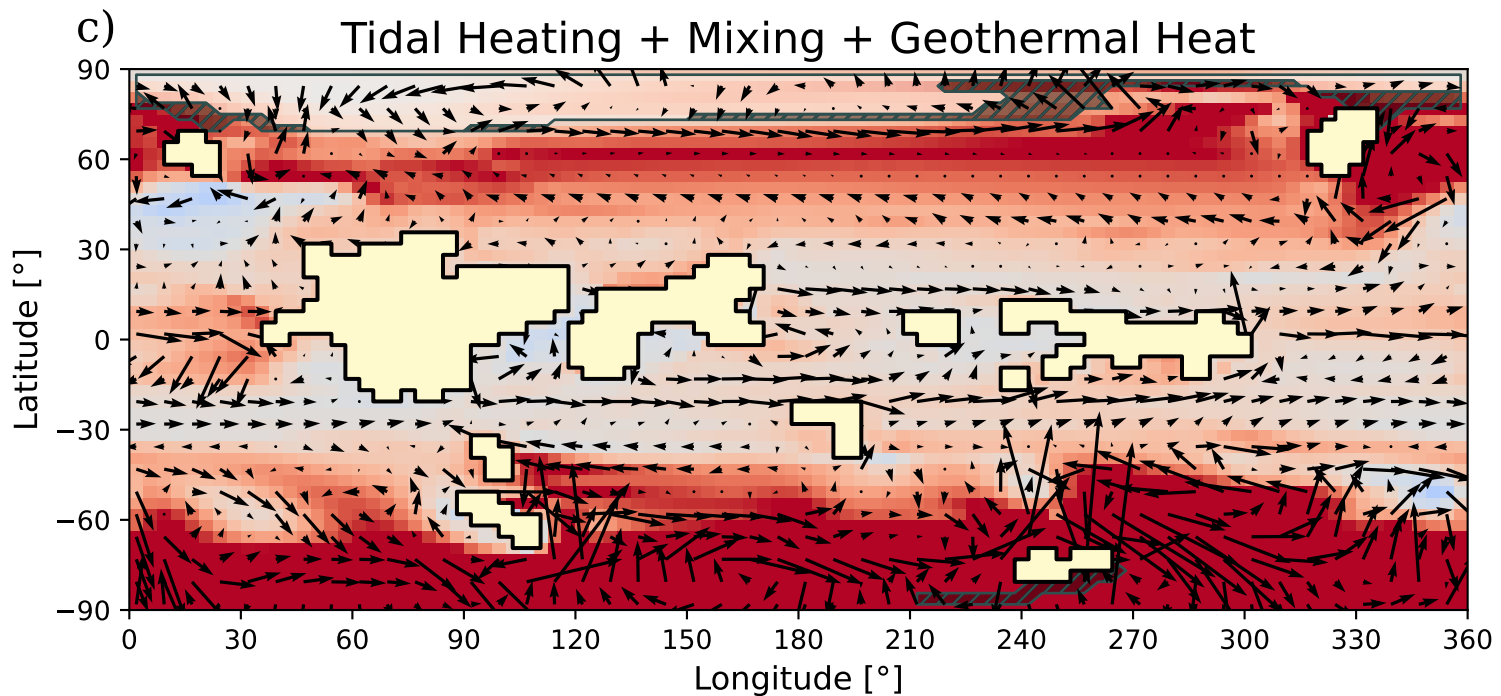
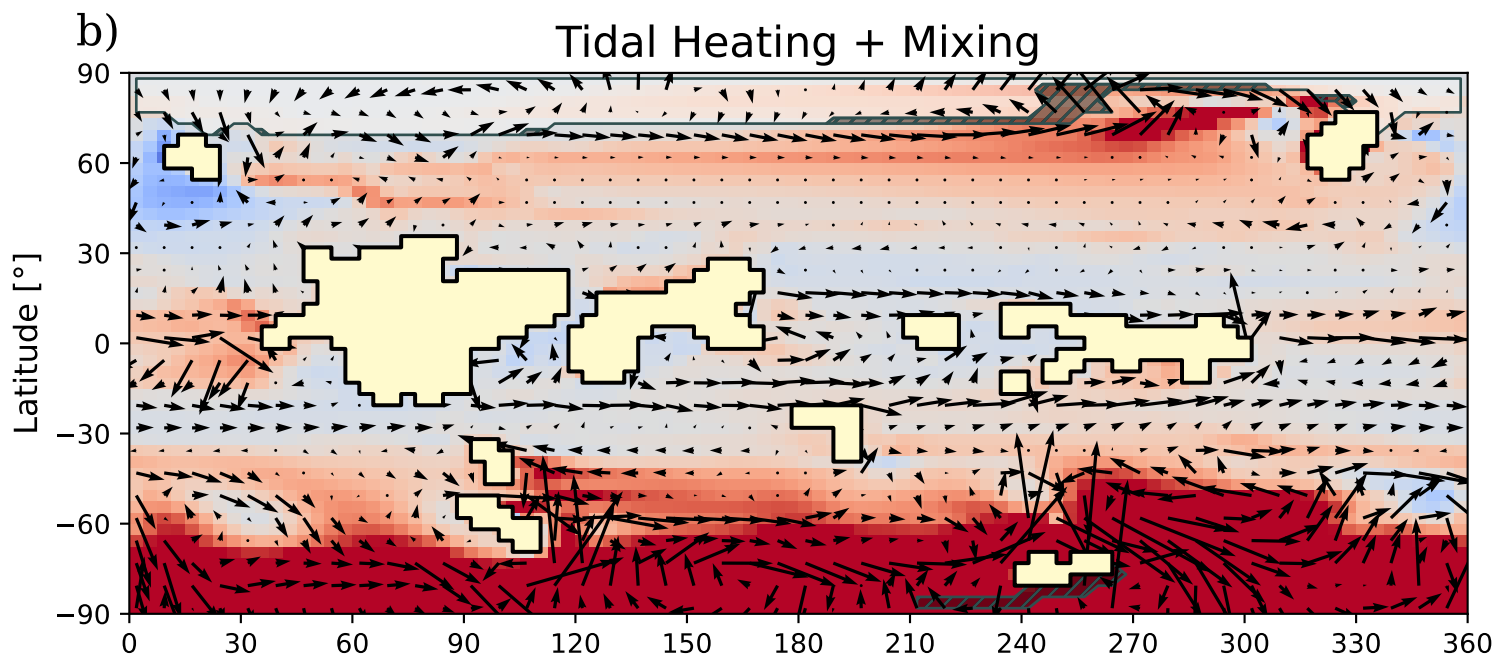
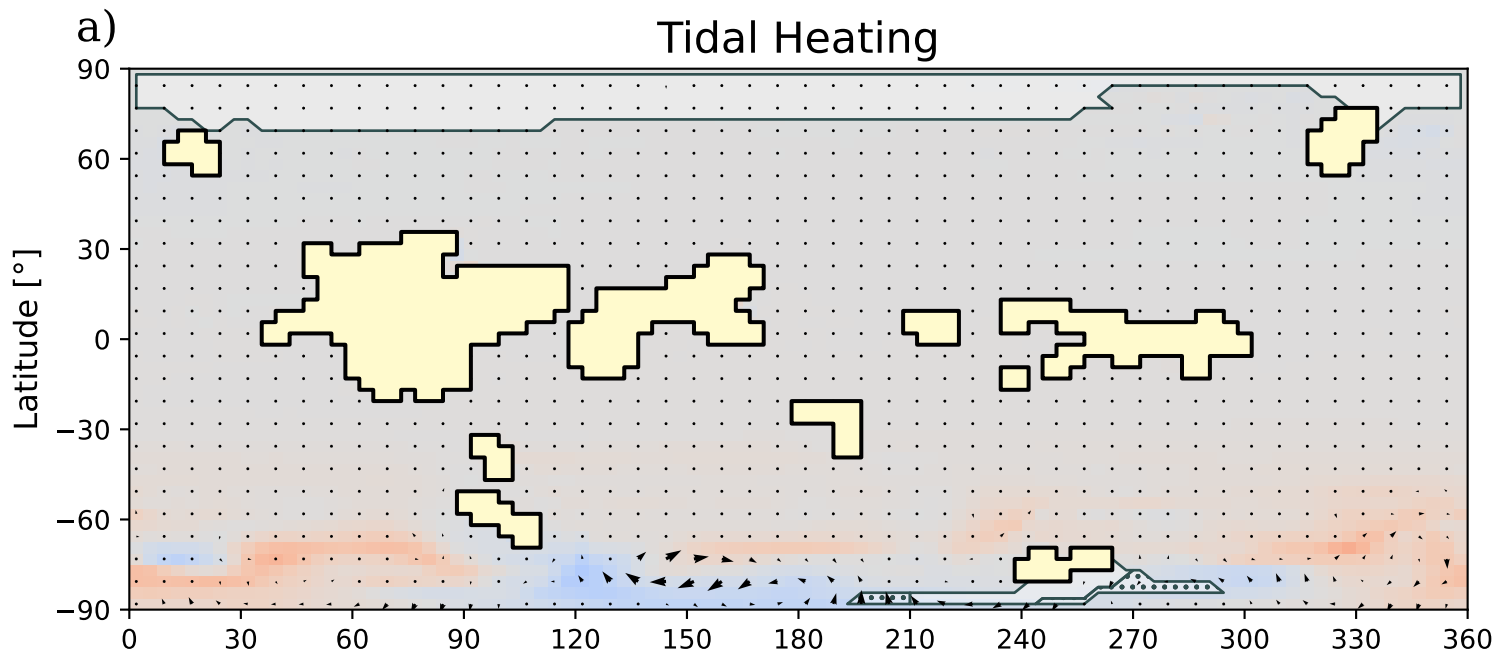


Figure 7.

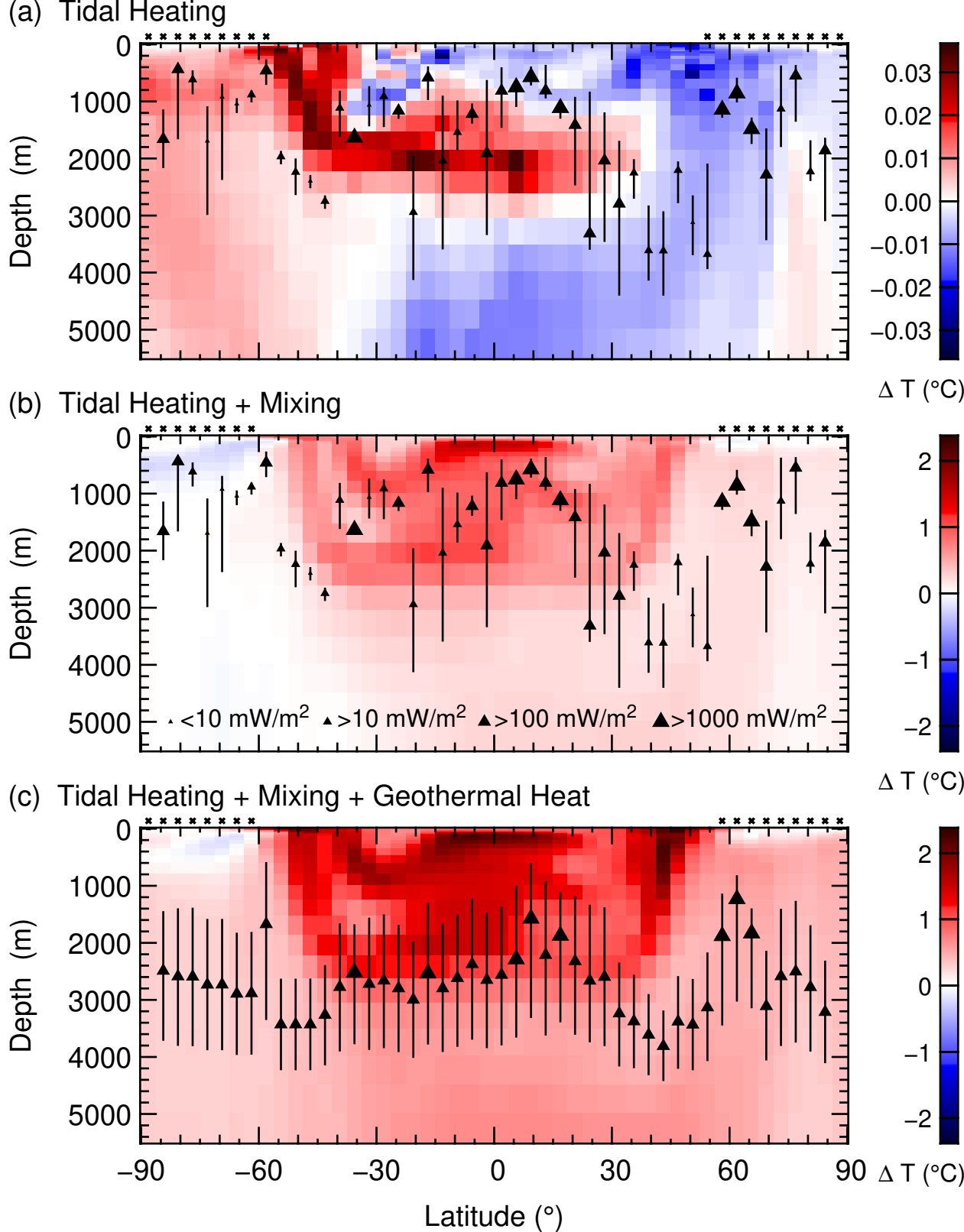
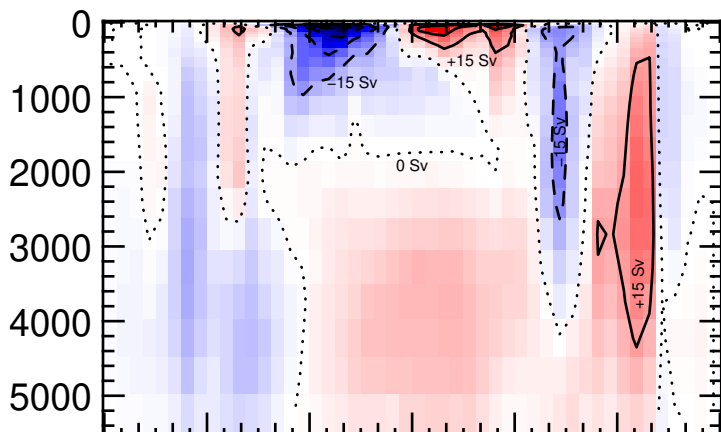
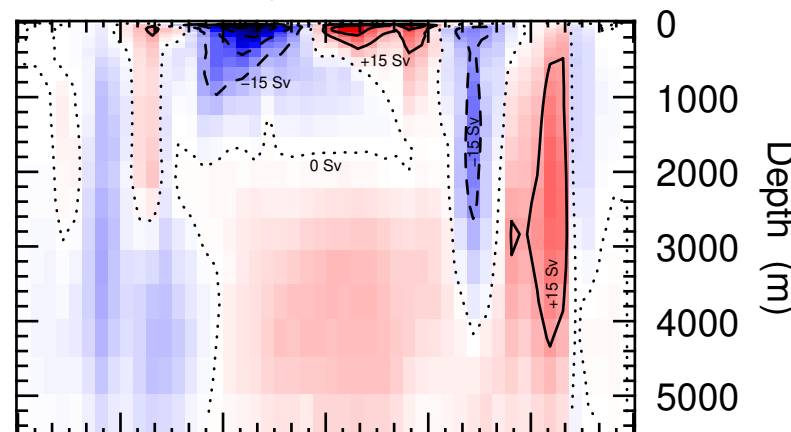


Figure 8.

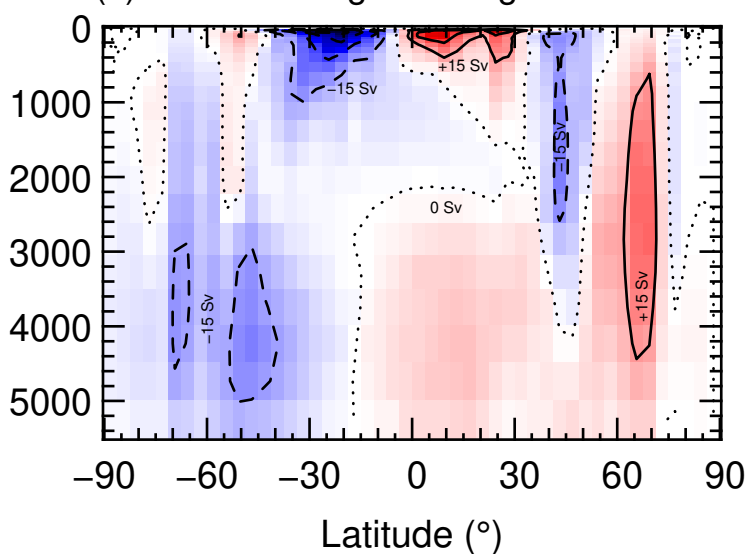
(a) Control



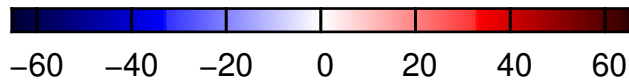
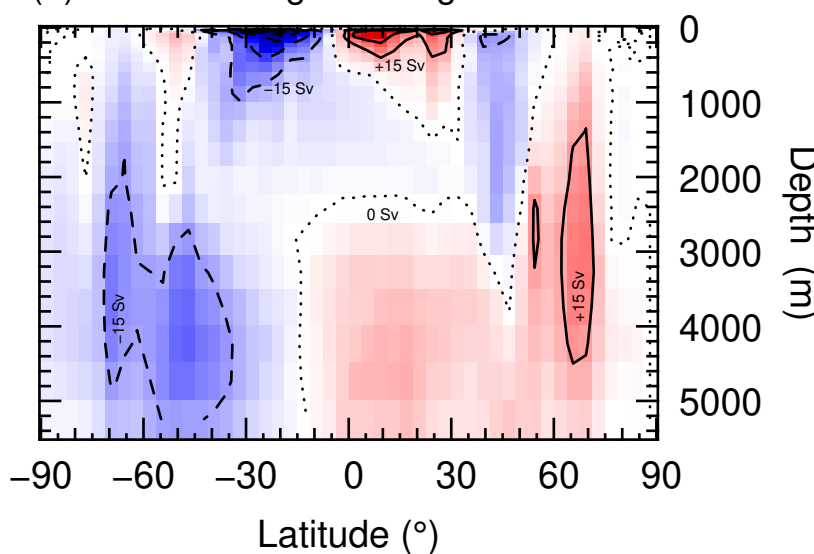
(b) Tidal Heating



(c) Tidal Heating + Mixing



(d) Tidal Heating + Mixing + Geothermal Heat



Overturning Streamfunction (Sv)

Figure B1.

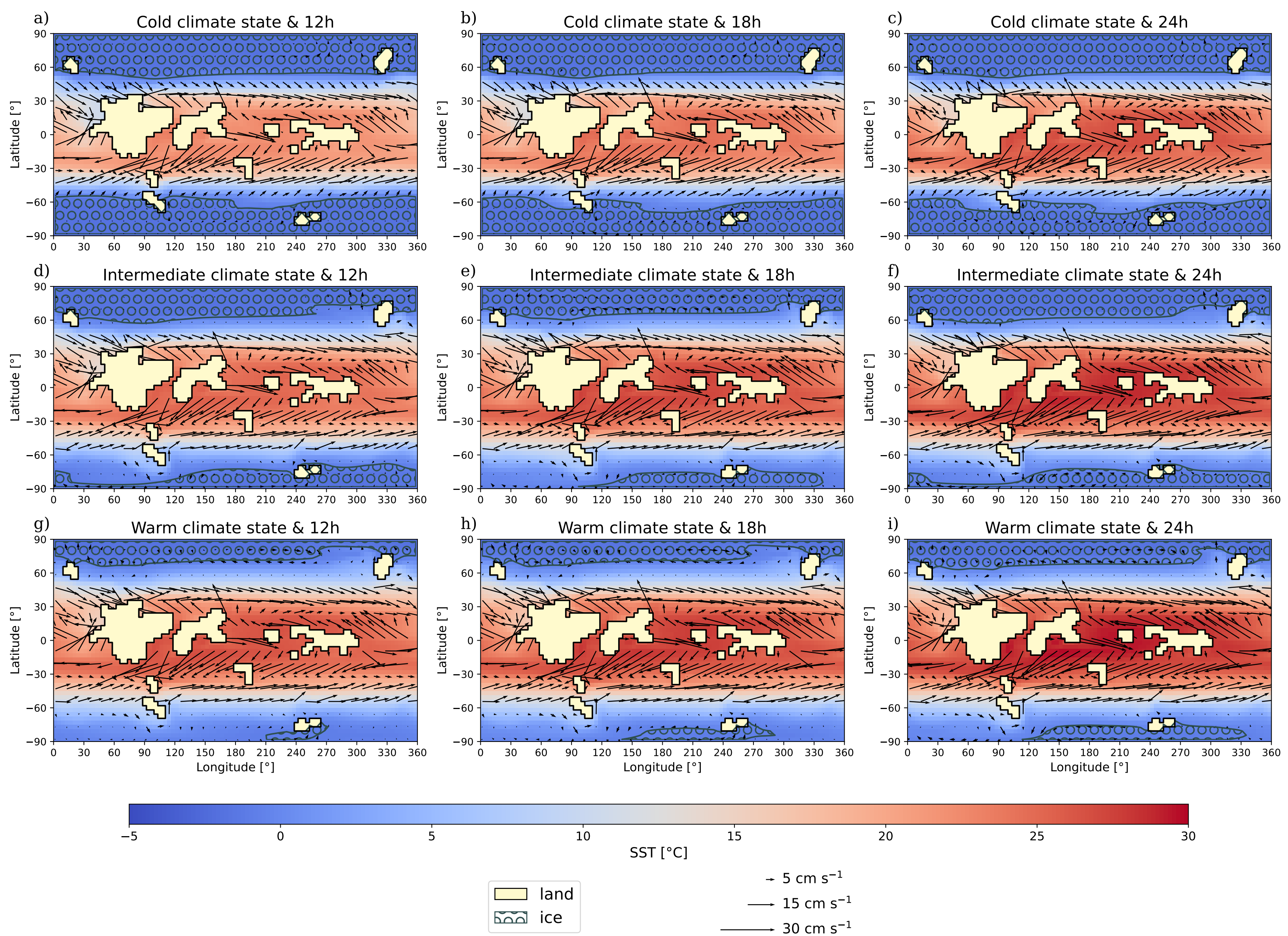


Figure B2.

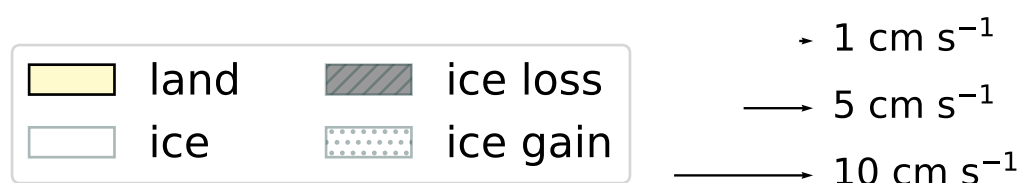
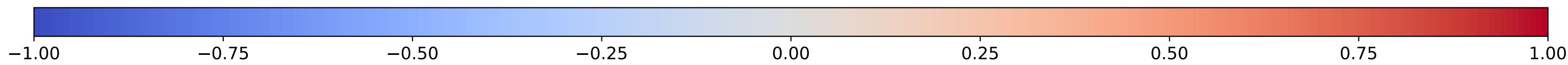
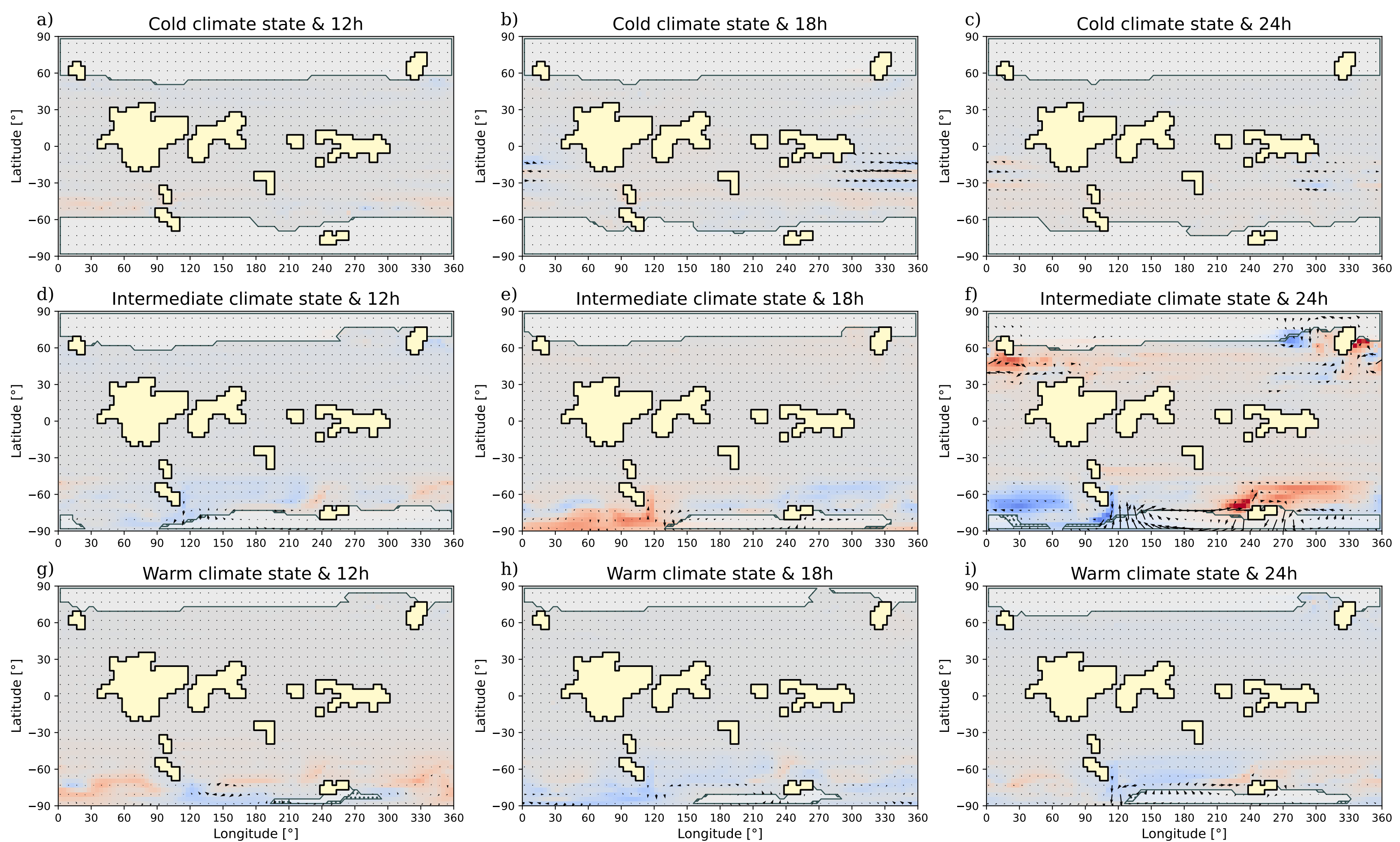


Figure B3.

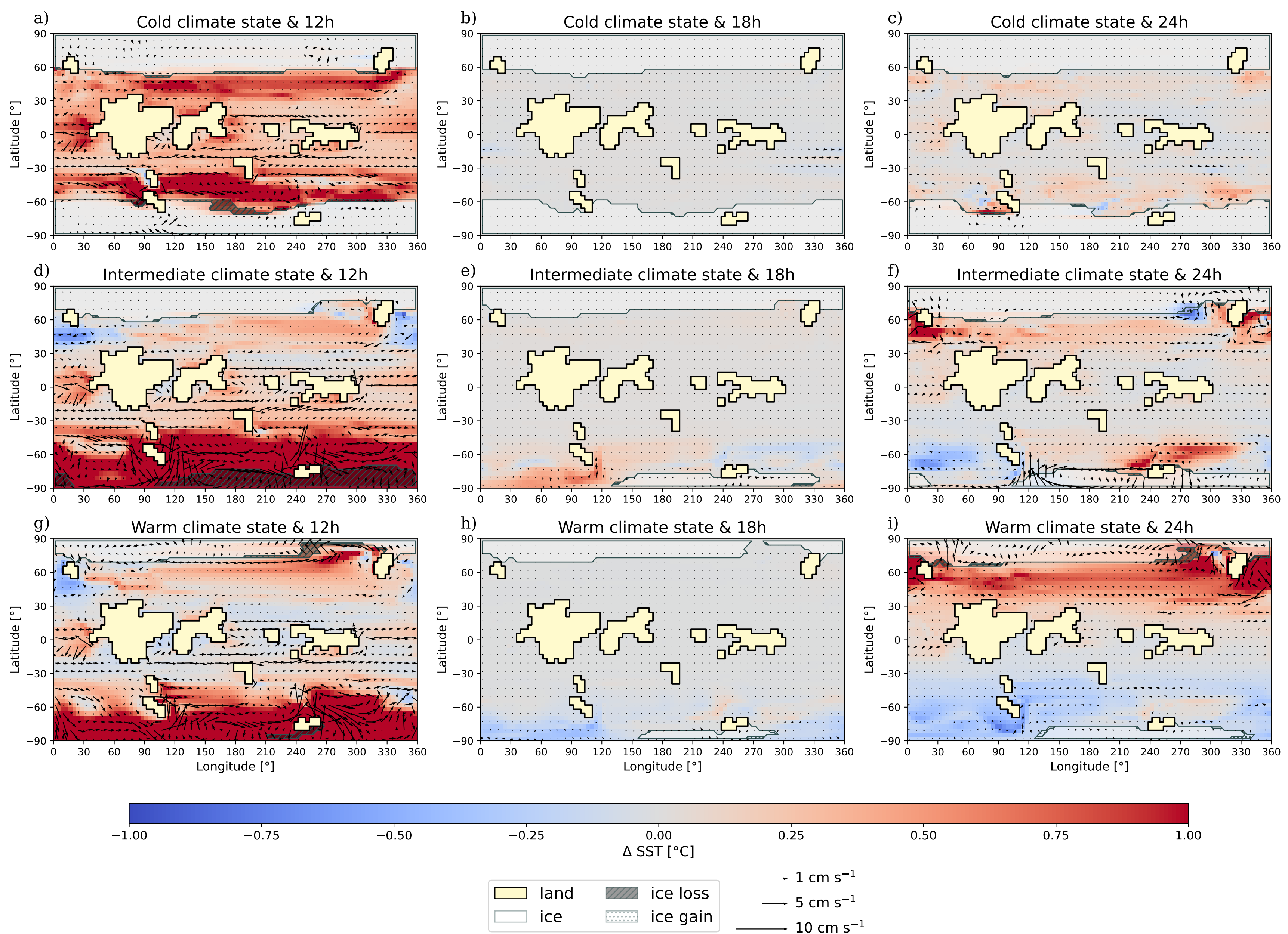


Figure B4.

